NASA TECHNICAL MEMORANDUM

NASA TM X- 62,354

NASA TM X-62,354

MAGNETISM AND THE INTERIOR OF THE MOON

Palmer Dyal, Curtis W. Parkin, and William D. Daily

Ames Research Center
Moffett Field, Calif. 94035

University of Santa Clara
Santa Clara, Calif. 95053

and

Brigham Young University
Provo, Utah 84602

February 1974

MAGNETISM AND THE INTERIOR OF THE MOON

by

Palmer Dyal
NASA-Ames Research Center
Moffett Field, California 94035

Curtis W. Parkin
Department of Physics, University of Santa Clara
Santa Clara, California 95053

William D. Daily
Department of Physics and Astronomy, Brigham Young University
Provo, Utah 84602

Short title: Magnetism and the Lunar Interior

ABSTRACT

During the time period 1961-1972 eleven magnetometers were sent to the moon. The primary purpose of this paper is to review the results of lunar magnetometer data analysis, with emphasis on the lunar interior. Magnetic fields have been measured on the lunar surface at the Apollo 12, 14, 15, and 16 landing sites. The remanent field values at these sites are respectively 38 γ, 103 γ (maximum), 3γ, and 327γ (maximum). Simultaneous magnetic field and solar plasma pressure measurements show that the Apollo 12 and 16 remanent fields are compressed during times of high plasma dynamic pressure. Apollo 15 and 16 subsatellite magnetometers have mapped in detail the fields above portions of the lunar surface and have placed an upper limit of 4.4×10^{13} gauss-cm^3 on the global permanent dipole moment. Satellite and surface measurements show strong evidence that the lunar crust is magnetized over much of the lunar globe. Magnetic fields are stronger in highland regions than in mare regions, and stronger on the lunar far side than on the near side. The largest magnetic anomaly measured to date is between the craters Van de Graaff and Aitken on the lunar far side. The origin of the lunar remanent field is not yet satisfactorily understood; several source models are presented. Simultaneous data from the Apollo 12 lunar surface magnetometer and the Explorer 35 Ames magnetometer are used to construct a whole-moon hysteresis curve, from which the global lunar permeability is

determined to be $\mu = 1.012 \pm 0.006$. The corresponding global induced dipole moment is $\sim 2 \times 10^{18}$ gauss-cm^3 for typical inducing fields of 10^{-4} gauss in the lunar environment. From the permeability measurement, lunar free iron abundance is determined to be 2.5 ± 2.0 wt. %. Total iron abundance (sum of iron in the ferromagnetic and paramagnetic states) is calculated for two assumed compositional models of the lunar interior. For a free iron/orthopyroxene lunar composition the total iron content is 12.8 ± 1.0 wt. %; for a free iron/olivine composition, total iron content is 5.5 ± 1.2 wt. %. Other lunar models with a small iron core and with a shallow iron-rich layer are also discussed in light of the measured global permeability. Global eddy current fields, induced by changes in the magnetic field external to the moon, have been analyzed to calculate lunar electrical conductivity profiles using several different analytical techniques. From nightside transient data with the moon in the solar wind, it has been found that deeper than 170 km into the moon, the conductivity rises from 3×10^{-4} mhos/meter to 10^{-2} mhos/meter at 1000 km depth. Harmonic analyses of dayside data differ from nightside results primarily at the greater lunar depths, where harmonic dayside profiles show lower conductivities than do the nightside results. Recent conductivity analysis of transients in the geomagnetic tail avoids many of the analytical problems posed by asymmetric confinement of induced fields

in the solar wind. A conductivity profile calculated from geomagnetic tail transient analysis, increases with depth from 10^{-9} mhos/meter at the lunar surface to 10^{-4} mhos/meter at 340 km depth, then to 2×10^{-2} mhos/meter at 870 km depth. This conductivity profile is converted to temperature and compared with temperature results of other investigators.

CONTENTS

I. Introduction

II. Lunar Magnetometers and the Lunar Magnetic Environment

A. The Lunar Magnetometers

B. The Lunar Magnetic Environment

III. Lunar Remanent Magnetic Fields

A. Surface Site Field Measurements

B. Orbital Field Measurements

C. Origin of the Lunar Remanent Magnetization

1. Large Solar or Terrestrial Field

2. Iron Core Dynamo

3. Ancient Magnetized Core

4. Shallow Fe-FeS Dynamo

5. Local Induced Unipolar Dynamo

6. Local Thermoelectrically Driven Dynamo

7. Shock Magnetization

8. Local Currents from Charged Particle Transport

IV. Global Magnetization Induction: Magnetic Permeability and Iron Abundance

A. Global Magnetic Permeability

1. Early Results from Explorer 35 Measurements

2. Results from Simultaneous Apollo and Explorer 35 Measurements

B. Lunar Iron Abundance

C. Considerations of an Iron Core and Iron-Rich Layer

V. Global Eddy Current Induction: Electrical Conductivity and Temperature

A. Electrical Conductivity Analysis: Moon in Solar Wind Plasma

1. Lunar Nightside Data Analysis: Transient Response

2. Lunar Dayside Data Analysis: Transient Response

3. Lunar Dayside Data Analysis: Harmonic Response

B. Electrical Conductivity Analysis: Moon in the Geomagnetic Tail

1. Poloidal Response of a Sphere in a Vacuum: Theory

2. Conductivity Results: Geomagnetic Tail Data Analysis

C. Lunar Temperature Profiles from Conductivity Analyses

VI. Summary

A. Lunar Remanent Magnetic Fields

B. Lunar Magnetic Permeability and Iron Abundance

C. Lunar Electrical Conductivity and Temperature

References

I. INTRODUCTION

Magnetometers placed on the lunar surface and in orbit about the moon have returned a wealth of information about the moon which was not anticipated prior to the Apollo manned lunar missions. Earlier measurements, by USSR and U.S. magnetometers on unmanned spacecraft, indicated that the moon might be electromagnetically inert; during that time investigators often concentrated on the interactions of the moon with the solar wind plasma (Colburn et al., 1967; Ness et al., 1967; Michel, 1968; Spreiter et al., 1970) rather than on magnetic studies of the lunar interior.

The measurement of magnetic fields in the vicinity of the moon began in January 1959, when the USSR spacecraft Luna 1 carried a magnetometer to within several hundred kilometers of the moon. In September 1959, Luna 2, also equipped with a magnetometer, impacted the lunar surface. The instrument aboard Luna 2 set an upper limit of 100 gammas (1 gamma = 10^{-5} gauss) for a possible lunar field at an altitude of about 50 km above the moon's surface (Dolginov, 1961). In April 1966, Luna 10, carrying a magnetometer 10 times more sensitive than that aboard Luna 2, was successfully placed in a lunar orbit that came to within 350 km of the moon (see Figure 1). The Luna 10 magnetometer recorded a time-varying magnetic field in the vicinity of the moon which was at that time interpreted as indicating the existence of a weak lunar magneto-

sphere (Dolginov et al., 1966).

A year later (July 1967) the United States placed the Explorer 35 satellite, with two magnetometers aboard, in orbit around the moon. In its orbit the satellite passes to within 830 km of the moon's surface. Explorer 35 successfully measured magnetic properties of the solar-wind cavity downstream from the moon, but it did not detect the lunar magnetosphere indicated by Luna 10 measurements nor the lunar bow shock and induced-field configuration previously suggested by Gold (1966). In an analysis of the Explorer 35 results Sonett et al. (1967) concluded that if a permanent lunar field exists at all, its magnitude would be less than two gammas at an altitude of 830 km and therefore ≤ 4 gammas at the surface for a global permanent dipole field. The upper limit on the global permanent dipole moment was set at 10^{20} gauss-cm^3, i.e., less than 10^{-5} that of the earth. In studies of the solar wind interaction with the lunar body (Colburn et al., 1967, Ness et al., 1967), investigators found the solar wind field magnitude to be $\sim$1.5 gammas greater in the diamagnetic cavity on the moon's antisolar side than in the solar wind.

Surveyor spacecraft, used in the first U.S. unmanned lunar landings, carried no magnetometers. Permanent magnets were carried aboard the Surveyor 5 and 6 spacecraft, however, which demonstrated that soils at those two landing sites contain less than

1% (by volume) ferromagnetic iron (de Wys, 1968).

During the early manned Apollo missions it was determined that the moon is much more interesting magnetically than had been expected. Natural remanent magnetization in lunar samples was found to be surprisingly high at all U.S. Apollo sites and at the USSR Luna 16 site (see, for example, Strangway et. al., 1970; Runcorn et al., 1970; Pearce et al., 1971; Nagata et al., 1971; Nagata et al., 1972b; Collinson et al., 1973; Pearce et al., 1973). Such high natural remanent magnetism implies that at some time in the past there existed an ambient surface magnetic field considerably higher than that which now exists on the moon (Runcorn et al., 1970; Gose et al., 1972).

The first lunar surface magnetometer (LSM), deployed at the Apollo 12 site in November 1969, made the first direct measurement of an intrinsic lunar magnetic field (Dyal et al., 1970a). The 38-gamma field measurement showed that not only are individual rocks magnetized, but also that magnetization in the lunar crust can be ordered over much larger regions, of 2 km to 200 km scale sizes (Dyal et al., 1970a; Barnes et al., 1971). The permanent and induced fields measured by the Apollo 12 magnetometer provided the impetus to develop portable surface magnetometers and subsatellite magnetometers for later Apollo missions. Permanent magnetic fields were subsequently measured at four other landing

sites: Apollo 14 (103 γ maximum), Apollo 15 (3 γ), Apollo 16 (327 γ maximum), and more recently at several positions along the USSR Lunakhod II traverse. The surface fields were attributed to local magnetized sources ("magcons"); their discovery prompted a reexamination of Explorer 35 magnetometer data by Mihalov et al., (1971), who found indirect evidence that several magnetized regions exist in the lunar crust. Direct field measurements from Apollo 15 and 16 subsatellite magnetometers, activated in August 1971 and April 1972, respectively, yielded maps of some of the larger magnetized regions in the lunar crust (Coleman et al., 1972c; Sharp et al., 1973) which confirmed the existence of magnetized regions over much of the lunar surface. Subsatellite magnetometer measurements have also placed an upper limit of 4.4×10^{13} gauss-cm^3 on the global permanent magnetic dipole moment (Russell et al., 1973).

Investigations of simultaneous surface magnetometer data and solar wind spectrometer data show that the surface remanent magnetic fields interact with the solar wind when on the dayside of the moon (Dyal et al., 1972[a]; Clay et al., 1972; Dyal and Parkin, 1971[b]). The interaction is interpreted as a compression of the surface remanent fields by the solar wind; the magnetic pressure at the surface increases in proportion to the dynamic bulk pressure of the solar wind plasma.

In addition to measuring permanent lunar fields, the network of lunar surface and orbiting magnetometers measured fields induced in the lunar interior by extralunar magnetic fields, allowing investigation of deep interior properties of the moon. Behannon (1968) placed an upper limit of 1.8 on the bulk relative magnetic permeability by studying Explorer 35 magnetometer measurements in the geomagnetic tail. Subsequently, simultaneous measurements of Explorer 35 and Apollo 12 magnetometers have been used to yield the more accurate value of 1.012 ± 0.006 (Parkin et al., 1974a,b). This permeability value has been used to calculate free iron and total iron abundance of the moon.

The electrical conductivity of the lunar interior has been investigated by analyzing the induction of global lunar fields by time-varying extralunar (solar or terrestrial) magnetic fields. Since temperature and conductivity of geological materials are related, calculated conductivity profiles have been used to infer temperature of the lunar interior. Early estimates of bulk lunar electrical conductivity were made from lunar-orbiting Explorer 35 data by Colburn et al., (1967) and Ness (1968). For homogeneous-conductivity models of the moon, Colburn et al. placed an upper limit of 10^{-6} mhos/m for whole-moon conductivity, whereas Ness' upper limit was 10^{-5} mhos/m. These investigators also stated that their measurements were consistent with higher conductivity

for a lunar core surrounded by an insulating crust.

Theoretical studies of the electrodynamic response of the moon to time-dependent external fields have been undertaken by many authors. Two types of whole-moon magnetic induction fields have been treated; a poloidal field due to eddy currents driven by time-varying external magnetic fields, and a toroidal field due to unipolar currents driven through the moon by the motional solar-wind $\underline{V} \times \underline{B}$ electric field.

The toroidal induction mode, first suggested to be an important process in the moon by Sonett and Colburn (1967), was later developed in detail theoretically for a lunar model totally confined by the highly conducting solar wind (Schwartz and Schubert, 1969; Schubert and Schwartz, 1969; Sill and Blank, 1970). However, analysis of simultaneous Apollo 12 and Explorer 35 magnetometer data later indicated that for the moon, toroidal induction is negligible in comparison to poloidal induction; upper limits on the toroidal field mode were used to calculate an upper limit of 10^{-9} mhos/m for electrical conductivity of the outer 5 km of the lunar crust (Dyal and Parkin, 1971a). In subsequent analysis of lunar electromagnetic induction, toroidal induction has been assumed to be negligible relative to poloidal induction.

The eddy-current response of a homogeneous sphere in a vacuum to time-varying magnetic fields has been described by Smythe (1950)

and Wait (1951). Early theoretical application of vacuum poloidal induction to studies of the lunar interior were presented by Gold (1966) and Tozer and Wilson (1967). Poloidal response theory for a lunar sphere totally confined by a highly conducting plasma was developed by Blank and Sill (1969), Schubert and Schwartz (1969), and Sill and Blank (1970).

Since deployment of the Apollo 12 magnetometer in November 1969, electrical conductivity analysis has been developed with two basic approaches: a time-dependent, transient- response technique (Dyal and Parkin, 1971c; Sill, 1972; Dyal et al., 1973) and a frequency-dependent, Fourier-harmonic technique (Sonett et. al., 1971, 1972; Kuckes, 1971; Sill, 1972; Hobbs, 1973). Past analyses have all used magnetometer data recorded at times when global eddy current fields were asymmetrically confined by the solar wind plasma (Reisz et al., 1972; Dyal and Parkin, 1973; Dyal et al., 1973; Schubert et al., 1973c; Smith et al., 1973). The asymmetric confinement of lunar fields is particularly complex to model theoretically (Schubert et al., 1973b); indeed, the general time-dependent asymmetric induction problem has not been solved at the time of this writing. To avoid these complications, recent conductivity analysis has used field data recorded in the geomagnetic tail, which is relatively free of plasma and asymmetric confinement effects. Preliminary results of this analysis will be pre-

sented in this paper.

The purpose of this paper is to review the application of lunar magnetic field measurements to the study of properties of the lunar crust and deep interior. Following a brief descriptive section on lunar magnetometers and the lunar magnetic environment, measurements of lunar remanent fields and their interaction with the solar plasma will be discussed. Then the magnetization induction mode will be considered with reference to lunar magnetic permeability and iron abundance calculations. Finally, electrical conductivity and temperature calculations from analyses of poloidal induction, for data taken in both the solar wind and in the geomagnetic tail, will be reviewed.

II LUNAR MAGNETOMETERS AND THE LUNAR MAGNETIC ENVIRONMENT

A. The Lunar Magnetometers

A network of three lunar surface magnetometers has been placed on the moon by astronauts on the Apollo 12, 15, and 16 missions. The vector magnetic field is measured three times per second and transmitted to earth from each of these three Apollo sites shown in Figure 1. Magnetometers in lunar orbit on board the Explorer 35 satellite (Sonett et. al., 1967) and on Apollo 15 and 16 subsatellites (Coleman et al., 1972a,b) measure the field external to the moon and transmit this information to earth. Also, portable magnetometers have been used by the astronauts at the Apollo 14 and 16 sites, to measure remanent fields at different locations along a surface traverse.

The stationary lunar surface magnetometer (LSM) deployed at the Apollo 12 site on the moon is shown in Figure 2. Similar magnetometers have been placed at the Apollo 15 and 16 sites. The three orthogonal vector components of the lunar surface magnetic field are measured by three fluxgate sensors (Gordon et al., 1965) located at the ends of three 100-cm-long orthogonal booms. The sensors are separated from each other by 150 cm and are 75 cm above the ground. The analog output of each sensor is internally processed by a low-pass digital filter and a telemetry encoder,

and the output is transmitted to earth via the central station S-band transmitter. The magnetometer has two data samplers, the analog-to-digital converter (26.5 samples/second) and the central station telemetry encoder (3.3 samples/second). The prealias filter following the sensor electronics has attenuations of 3 dB at 1.7 Hz and 58 dB at the Nyquist frequency (13.2 Hz), with an attenuation rate of 22 dB/octave. The four-pole Bessel digital filter has an attenuation of 3 dB at 0.3 Hz and 48 dB at the telemetry sampling Nyquist frequency (1.6 Hz). Instrument resolution is 0.2 γ. The instrument is also used as a gradiometer by sending commands to operate three motors in the instrument which rotate the sensors such that all simultaneously align parallel first to one of the boom axes, then to each of the other two boom axes in turn. This sensor alignment permits the vector gradient to be calculated in the plane of the sensors and also permits an independent measurement of the magnetic field vector at each sensor position. A detailed description of the stationary magnetometer is reported by Dyal et al., (1970b).

The lunar portable magnetometer (LPM) was developed for astronaut deployment on the Apollo 14 and 16 missions (the Apollo 16 LPM is shown in Figure 3b). The instrument was designed to be a totally self-contained, portable experiment package. Three

orthogonally oriented fluxgate sensors are mounted on the top of a tripod, positioned 75 cm above the lunar surface. These sensors are connected by a 15-meter-long cable to an electronics box which contains a battery, electronics, and three field component readouts (meters on Apollo 14 LPM; digital displays on Apollo 16 LPM). The electronics box is mounted on the mobile equipment transporter for Apollo 14 and on the lunar roving vehicle for Apollo 16. Portable magnetometer measurements can be made only by manual activation by an astronaut. Instrument resolution is 1γ or 2 γ for the Apollo 14 LPM and 0.2γ for the Apollo 16 LPM. Detailed instrument characteristics are reported by Dyal et al. (1972c).

Magnetic fields of the lunar environment are measured by the Explorer 35 satellite magnetometers. The satellite, launched in July 1967, has an orbital period of 11.5 hours, aposelene of 9390 km, and periselene of 2570 km. Two magnetometers are carried aboard Explorer 35, one provided by NASA-Ames Research Center and the other provided by NASA-Goddard Space Flight Center. Since most of the analysis of lunar internal properties has been carried out using the Ames magnetometer, its characteristics will be considered here. The Explorer 35 Ames magnetometer measures three magnetic field vector components every 6.14 sec at 0.4 γ resolution; the instrument has an alias filter with 18 dB attenu-

ation at the Nyquist frequency (0.08 Hz) of the spacecraft data sampling system. A more detailed description of the instrument is reported by Sonett et al. (1967b).

The Apollo 15 (Figure 3a) and 16 subsatellite magnetometers, which orbited approximately 100 km above the lunar surface, also measured fields intrinsic to the moon. The subsatellite period of revolution is 2 hours. The subsatellite realtime sampling rates are 1 per 2 seconds for the field component along the spacecraft spin axis and 1 per second for the field component in the spin plane. Storage rates (for fields measured when the subsatellite is behind the moon relative to earth) are 1 field vector per 12 seconds (high rate) or 1 vector per 24 seconds (low rate). Apollo 15 resolution is 0.4γ or 1.6γ, depending on range; Apollo 16 resolution is 0.2γ or 0.8γ. The subsatellite magnetometer characteristics are described in detail by Coleman et al. (1972 a,b). At the time of this writing, the Apollo 16 lunar surface magnetometer (LSM) is the only lunar surface/or orbital magnetometer which is still returning useful scientific data.

B. The Lunar Magnetic Environment

In different regions of a lunar orbit, the magnetic environment of the moon can have distinctly different characteristics (see Figure 4). Average magnetic field conditions vary from relatively steady fields of magnitude $\sim 9\gamma$ in the geomagnetic tail to mildly turbulent fields averaging $\sim 5\gamma$ in the free-streaming solar plasma region to turbulent fields averaging $\sim 8\gamma$ in the magnetosheath. Average solar wind velocity is $\sim$400 km/sec in a direction approximately along the sun-earth line.

The interaction of the solar wind with the earth's permanent dipole field results in formation of the characteristic shape of the earth's magnetosphere; the solar wind in effect sweeps the earth's field back into a cylindrical region (the geomagnetic tail) on the earth's antisolar side. The earth's field magnitude is about 30,000γ at the equator; in the geomagnetic tail the field decreases with distance from the earth with a radial dependence expressible as $R^{-0.736}$ (Mihalov et al., 1968). At the distance where the moon's orbit intersects the tail, the field magnitude is $\sim$10 gammas. The moon is in the geomagnetic tail for about four days of each 29.5-day lunation (period between successive full moons). Substructure of the tail consists of two "lobes": the upper or northward lobe has its magnetic field pointing roughly toward the earth, whereas the lower lobe field points away from

the earth. The moon can pass through either or both lobes, depending upon the characteristics of the particular orbit, the geomagnetic dipole axis orientation, and perturbations of the geomagnetic field by solar wind pressures.

The total magnetic field at the lunar surface is the vector sum of the following fields: the external (solar or terrestrial) "driving" field, permanent and induced lunar fields, and fields associated with the moon-plasma interaction in the solar wind. The lunar orbiting Explorer 35 magnetometer measures the external driving field. Analysis of these external "input" fields and the corresponding surface "response" fields allows calculation of properties of the lunar interior such as magnetic permeability, iron abundance, electrical conductivity, and temperature. The solar plasma interaction with lunar surface remanent fields is studied by correlating field data with plasma measurements.

Since the external driving magnetic field in the lunar environment can vary considerably with the lunar orbital position (see Figure 4), it is possible to study different lunar properties in different regions of the lunar orbit. A particular property of the moon is analyzed by selecting the lunar environment most favorable for induction of a lunar field response which is functionally dependent upon that particular property. During times when

the moon is immersed in the steady geomagnetic tail field, time-dependent induction fields and solar wind interaction fields are minimal. This condition allows investigation of lunar permanent fields and time-independent magnetization ("soft perm") fields; the latter are functions of lunar magnetic permeability. When the moon is immersed in the variable fields of the free streaming solar wind or the magnetosheath, poloidal induction is the dominant lunar response field. In the past, investigators have used data taken in these regions of the orbit to study electrical conductivity. More recent analyses have used magnetic field data measured in the geomagnetic tail, where plasma effects are minimized, in order to avoid complications due to asymmetric plasma confinement.

III. LUNAR REMANENT MAGNETIC FIELDS

The permanent magnetic fields of the moon have been investigated using surface magnetometer measurements at four Apollo sites and one USSR Luna site; orbital measurements from Explorer 35 and two Apollo subsatellite magnetometers; and natural remanent magnetization measurements of returned lunar samples. Lunar remanent field measurements by surface and orbiting magnetometers will be emphasized in this paper. Sample magnetization measurements have been reviewed elsewhere (Hinners, 1971; Nagata et al., 1972a; Strangway et al., 1973c; Fuller, 1974).

A. Surface Site Field Measurements

The permanent magnetic fields of the moon were first measured in situ by the Apollo 12 lunar surface magnetometer (LSM) which was deployed on the eastern edge of Oceanus Procellarum. The permanent field magnitude was measured to be 38 $\pm$ 3 gammas and the source of this field was determined to be local in extent (Dyal et al., 1970a; Barnes et al., 1971; see Figure 5). A remanent field this large was generally unexpected even in light of the NRM discovered in the Apollo 11 samples, and the explanation of its origin yet remains a central problem in lunar magnetism. Subsequent to this measurement of an intrinsic lunar magnetic field, surface magnetometers have measured fields at the Apollo 14, 15 and 16 sites. Fields of 103 $\pm$ 5 and 43 $\pm$ 6 gammas, at two sites located about a

kilometer apart, were measured by the Apollo 14 Lunar Portable magnetometer (LPM) at Fra Mauro. (see Figure 6). A steady field of 3.4±2.9 gammas was measured near Hadley Rille by the Apollo 15 LSM (see Figure 7). At the Apollo 16 landing site both a portable and stationary magnetometer were deployed; magnetic fields ranging between 112 and 327 gammas were measured at five different locations over a total distance of 7.1 kilometers at the Descartes landing site. These are the largest lunar fields yet measured. A schematic representation of the measured field vectors is shown in Figure 8 . All the vectors have components pointing downward except the one at Site 5 near Stone Mountain, which points upward. This suggests among other possibilities, that the material underlying Stone Mountain has undergone different geological processes than that underlying the Cayley Plains and North Ray Crater. In fact, Strangway et al. (1973b) proposed the possibility that the light colored, relatively smooth Cayley formation is magnetized roughly vertically; the difference in the vertical component at site 5 was explained as an edge effect at the Cayley Plains-Stone Mountain boundary. A summary of all remanent lunar fields measured by the magnetometers deployed on the surface is given in Table 1.

Interaction of the solar wind with the remanent magnetic field has been measured at the Apollo 12 and 16 landing sites. The solar plasma is directly measured at the Apollo 12 and 15 sites (Clay et

al., 1972) and simultaneous magnetic field and plasma data show a compression of the steady field as a function of the solar wind pressure at the Apollo 12 and 16 sites (Dyal et al., 1973). The nature of the correlation between magnetic field and plasma bulk flow pressures is shown in Figure 9, which shows data (combined from several lunations) at the Apollo 12 and 16 LSM sites. The plasma bulk flow pressure and the magnetic pressure are related throughout the measurement range, and the magnitudes of magnetic pressure changes are in proportion to the unperturbed steady field magnitudes at each site.

Information on the scale sizes of the permanently magnetized regions near Apollo landing sites is given by gradient measurements of the lunar surface magnetometers, the spacing of vector measurements over the lunar surface, the known interaction properties of these remanent fields with the solar wind plasma, and limits imposed by satellite measurements. The field gradient in a plane parallel to the lunar surface is less than the instrument resolution of 0.13 gamma/meter at the Apollo 12 and 15 sites. At Apollo 14 a field difference of 60γ was measured at two sites located 1.1 km apart. Gradient measurements and the absence of changes in the permanent field at the sites after lunar module ascent demonstrated that the field sources are not magnetized artifacts.

The scale size of the Apollo 12 remanent field has been calcu-

lated from local gradient and Explorer 35 measurements to be from 2 km to 200 km (Dyal et al., 1972). For the Apollo 16 field, portable magnetometer measurements over the lunar roving vehicle traverse showed that the scale size for the field was greater than 5 km; the Apollo 16 subsatellite magnetometer showed no anomalous field attributable to the Descartes area at orbital altitude, implying a surface field scale size upper limit of 100 km. Therefore the Apollo 16 remanent field scale size is between 5 and 100 km.

B. Orbital Field Measurements

Remanent magnetic fields over extended regions of the surface have been studied using lunar orbiting magnetometers. Two techniques have been employed in these studies: measurement of the effects from the solar wind interaction with surface fields near the limb and direct measurement and mapping of the fields from orbit.

Interaction of the solar wind with certain regions near the limb of the moon were used to infer surface field strengths and scale sizes by Barnes et al. (1971) and Mihalov et al. (1971). Their techniques were based on the concept that the highly conducting solar wind plasma may interact with certain high field regions on the moon when the regions are near the limb, to produce a weak local shock or "limb compression". Such shocks could be detected downstream from the moon. Magnetic events in the Explorer 35 magnetometer data were interpreted by Mihalov et al. (1971) as evidence for these limb shocks and were also used to infer loca-

tions and relative field strengths of surface field concentrations. They concluded that there may be magnetic concentrations covering much of the lunar surface, with stronger concentrations on the lunar far side than on the near side and generally in highland rather than mare regions. Limb compressions have also been observed by the close orbiting Apollo 15 and 16 subsatellite magnetometers. Using data from these magnetometers Russell et al. (1973) have concluded that the source regions for the limb compressions tend to be concentrated in the lunar highlands and especially in the Tsiolkovsky area on the lunar far side. Limb shocks imply but do not confirm the existence of magnetized regions on the moon, since the exact mechanism for limb shock formation is not known and there are other possible causes for their formation such as crustal conductivity anomalies (Mihalov et al., 197/; Schubert et al., 1974) or solar wind interaction with irregularities in the lunar electron sheath near the limb (Criswell, 1973).

Direct measurements of the lunar surface fields have been made over about 5% of the lunar surface by the Apollo 15 and 16 subsatellite magnetometers (Coleman et al., 1972a,b). At the subsatellite altitudes of about 100 km the surface field magnitudes are generally less than 0.5 gamma (although sometimes they are as much as 2.5 gammas); by averaging data from several orbits which pass over the same surface area, measurements of the fields can be made along

the entire orbit. Then successive orbits can be combined to produce magnetic maps of the regions over which the satellite passes. Using an empirical relation between the height and strength of the field, the orbital values are then referenced to 100 km altitude and contours of equal intensity can be drawn for this altitude. The maps of lunar remanent magnetic field shown in Figures 10 through 13 were constructed using the first four lunations of Apollo 15 subsatellite data (Sharp et al., 1973). (The contour labels are in hundredths of gammas and a positive value indicates an outward directed field) The most obvious characteristic of these maps is the presence of significant lunar fields over most of the mapped regions. Apparently the remanent fields measured at the Apollo surface sites are not anomalous but rather, characteristic of remanent fields over much of the lunar surface. The contour spacing shows another important characteristic of the field: gradients are often relatively small over large distances, implying that some of the field sources are large-scale, i.e., that subsurface materials may be magnetized in a systematic manner over distances of tens to a few hundreds of kilometers. While these magnetized regions may be shallow, it is possible that lunar material is magnetized to a depth of tens or a few hundreds of kilometers, perhaps even down to the depth where the temperature rises to the iron Curie point. Contour lines of the subsatellite maps do not extend over

Fig. 10
11
12
13

the Apollo sites where fields have been measured at the surface. However, at both the Apollo 15 and 16 sites, near the map's perimeter, the field component normal to the surface as measured on the surface and at 100 km seem to be completely unrelated (compare Table 1 and Figure 12).

Comparison of the features in the orbital maps with surface geologic features has been of great interest, and some correlation has been found (Sharp et al., 1973). There is a marked nearside-farside asymmetry. The farside field is generally stronger and more structured than the nearside field. This observation may be due to concentration of source regions in lunar highlands and the asymmetric distribution of the highlands between the far and near side.

The most promonent magnetic feature measured to date by the subsatellite is located between the craters Aitken and Van de Graaff. This region has been mapped at altitudes of 67 km and 130 km. Most of the main features are qualitatively similar at the altitudes 67 km and 130 km, although more detailed structure in the contours is apparent at the lower altitude. Again there is a wide range of field source scale sizes which are likely in this area. Sharp et al. (1973) have estimated the size and magnetization of the principal source region. If the source is a thin circular disk 160 km across and 10 km thick it would require

a magnetization of nearly 7×10^{-5} emu/cm^3 to coincide with measurements. A magnetization typical of lunar samples is about 10^{-5} emu/cm^3. If the source region is a sphere instead of a disk, its center must be 75 km deep to yield the observed radial gradient. With a 10 km radius the magnetization would be 10^{-3} emu/cm^3, producing a 16 gamma surface field. A sphere 75 km in radius would require a magnetization intensity of 1.9×10^{-5} emu/cm^3. Other regions such as the Korolev, Hertsprung and Milne basins were also analyzed in some detail but the results were inconclusive due to unfavorable observational conditions and the smaller sizes of these features.

Some preliminary results from the Apollo 16 subsatellite magnetometer have been published (Sharp et al., 1973); as in the earlier experiment, the data indicate large-scale magnetic features in the lunar crust. The Apollo 16 subsatellite impacted the lunar surface shortly after the two passes of the moon through the geomagnetic tail, making available measurements from very low altitudes near periselene (10 to 0 km) during the last few orbits. Not only are the field magnitudes greatly enhanced (up to 56 gammas), but they change character over much smaller distances than those measured at 100 km. A wide range in field source sizes in the lunar crust is again indicated.

C. Origin of the Lunar Remanent Magnetization

From the beginning of the Apollo missions the origin of the lunar remanent fields has been of great interest. There has been no shortage of mechanism proposed to explain the origin of the lunar fields and remanence. Some of these possible mechanisms are discussed briefly here and displayed schematically in Figures 14 and 15.

1. Large Solar or Terrestrial Field. It has been proposed that the near-surface lunar material acquired a thermoremanence from cooling to the Curie point in the presence of a large solar or terrestrial field. One possibility is that the solar field was much stronger than it is now, and was also relatively steady during the rock crystallization (Nagata et al., 1972b). A terrestrial field increase greater than 100 times its present value would probably be necessary to magnetize lunar material at the present-day lunar orbit. Such a large terrestrial field is not indicated by paleomagnetic studies. For an ancient terrestrial field of present-day magnitude, the moon would have to have approached to within 2 to 3 Earth radii, close to the Roche limit (Runcorn et al., 1970; Helsley, 1970) to be subjected to the necessary field strength. All of the alternatives for these hypotheses seem to have shortcomings.

2. Iron Core Dynamo. For this mechanism a whole-moon field results from the self-generating dynamo action of a small iron core (Runcorn

et al., 1971; Strangway et al., 1971). The dynamo is assumed to have been active 3 to 4 billion years ago when surface rocks and breccias were formed. After the thermoremanent magnetization was established in the upper crust material, as it cooled through the Curie temperature, the dynamo turned off. Subsequently meteorite impacts on the magnetized surface randomized the field's sources by a gardening process and destroyed the whole-body magnetization in the crust. The core dynamo hypothesis also has its shortcomings. In the first place it is not clear that even the most efficient dynamo mechanism in a lunar core of limited size would be self sustaining at rotational speeds for which the moon could hold together (Levy, 1972). In addition, it is doubtful that a dynamo, if ever operating, could produce the surface fields to explain the thermal remanent magnetization of some lunar samples (Collinson et al., 1973; Levy, 1972).

Ancient Magnetized Core. Urey and Runcorn (1973) and Strangway et al. (1973a,c) have suggested that near surface material may have been magnetized by the field of a lunar core which had been previously magnetized by one of several possible means: (1) isothermally by a strong transient field, (2) viscous remanent magnetization by a weak field applied over a long period, (3) depositional remanent magnetization during early lunar formation in a weak field, or (4) thermoremanent magnetization of the core by cooling through

the Curie point in a weak field. If the moon formed in a cold state, neither accretion nor radioactivity would necessarily have raised the temperature of the deep interior above the Curie point of iron, with accompanying loss of magnetization, until 4.1 to 3.2 billion years ago. In the outer shell, perhaps 200 to 400 km thick, partial melting could easily have been realized during later stages of accretion. During the crystallization of the crustal rocks in the magnetic field of the core, they obtained a thermoremanence. Subsequently, radioactive heating in the interior raised the core temperature above the Curie point, resulting in loss of the magnetization in the core.

4. Shallow Fe-FeS Dynamos. A model related to the lunar core dynamo is one hypothesizing small pockets of iron and iron sulfide (Fe-FeS) melt a few hundred kilometers below the surface (Murthy and Banerjee, 1973) which act as small localized dynamos. The proponents of this mechanism suggest that these "fescons" are about 100 km in diameter. A variation of this local dynamo idea is suggested by Smolychowski (1973) wherein a thin layer of molten basalt generates the field. The existence of such local source regions for magnetic field should be evident once the surface fields have been mapped over more of the lunar surface. However, the recently discovered asymmetry in the electromagnetic field fluctuations at the Apollo 15 landing site (Schubert et al., 1974) could be due to such

a highly conducting subsurface body.

5. Local Induced Unipolar Dynamo. The solar wind transports magnetic fields past the moon at velocities $\underline{V}$ of approximately 400 km/sec; the corresponding $\underline{V} \times \underline{B}$ electric field causes currents to flow along paths of high electrical conductivity (Schwartz et al., 1969; Nagata et al., 1972b) such as molten mare regions, with the highly conducting solar wind plasma completing the circuit back to the lunar interior. The fields associated with these currents magnetize the materials as they cool below the Curie temperature. Because this induction mechanism has the strongest influence while the hot region is sunlit, an average preferred direction is associated with $\underline{V}$. However, the $\underline{V} \times \underline{B}$ induction model requires solar wind magnetic fields or velocities much higher than the present-day sun provides.

6. Local Thermoelectrically Driven Dynamo. Dyal et al. (1973) have proposed a mechanism of thermoelectrically driven currents to account for remanent fields. Thermoelectric potential is a function of the thermal gradient and electrical properties of the geological material. For the mechanism a mare basin is modeled by a disk which has an axial temperature gradient. Thermal gradients in the cooling mare lava could produce a Thomson thermoelectromotive force which would drive currents axially through the mare disk. The solar wind plasma, highly conducting along magnetic field lines, could provide a return path to complete the electrical circuit from

the top surface of the lava to the lunar surface outside the mare and back into the mare through the lunar interior. The upper limit of the fields generated in terrestrial materials by this process is a few thousand gammas. Such fields near a mare disk would produce thermoremanent magnetization in the moon of magnitudes measured in lunar samples. This mechanism awaits experimental verification using materials characteristic of lunar mare composition.

7. Shock Magnetization. Anisotropic compression of rocks by meteorite impacts is suggested by Nagata et al. (1970) as a means of inducing a remanence in certain samples which they studied magnetically. This piezo-remanent magnetization can be significantly large even when the external field is very weak (e.g., the solar wind field) if the uniaxial compression is very large. This mechanism is appealing since it relies on a well-established lunar process and may explain some correlation between craters and magnetic anomalies (Sharp et al., 1973), but the details remain undeveloped.

8. Local Currents from Charged Particle Transport. Any process which results in plasma flow near the lunar surface may generate strong local currents and magnetic fields. Cap (1972), for example, has shown that ionized volcanic ash flows may produce fields up to 10^3 gammas. As another example, Nagata et al. (1970) proposed the idea that lightning may be generated as a result of exploding dust clouds from meteorite impacts. The large currents

associated with an electrical discharge could produce transient magnetic fields up to 10 or 20 gauss, resulting in isothermal remanent magnetization of local material.

IV. GLOBAL MAGNETIZATION INDUCTION: MAGNETIC PERMEABILITY AND IRON ABUNDANCE

Magnetic permeability and iron abundance of the moon are calculated by analysis of magnetization fields induced in the permeable material of the moon. When the moon is immersed in an external field it is magnetized; the induced magnetization is a function of the distribution of permeable material in the interior. Under the assumption that the permeable material in the moon is predominately free iron and iron-bearing minerals, the lunar iron abundance can be calculated from the lunar permeability for assumed compositional models of the interior. Since the amount of iron present in the lunar interior should be consistent with the measured global magnetic permeability, the permeability in effect places a constraint on the physical and chemical composition of the moon's interior.

In this section calculations of global permeability will be reviewed, beginning with earlier measurements which used a single moon-orbiting magnetometer and proceeding chronologically to more recent studies using simultaneous data from surface and orbital magnetometers. More recent values of global permeability have been used to determine lunar iron abundance. This analysis of iron abundance and its implications concerning lunar composition and structure will be discussed.

A. Global Magnetic Permeability

1. Early Results from Explorer 35 Measurements. Behannon (1968) placed an upper limit on lunar bulk permeability using data from the Explorer 35 Goddard magnetometer. In his analysis, Behannon used data measured when the moon was in steady-field regions of the geomagnetic tail, where it was assumed that the external field was uniform over the region of space near the moon and plasma effects were negligible. Under these conditions, for a moon of spherically symmetric permeability distribution, the induced magnetization moment would be dipolar, with the dipole axis oriented along the external field. Behannon compared Explorer 35 field measurements made when the moon was above the neutral sheet (with the induced dipole oriented along the field pointing sunward) with those made when the moon was below the neutral sheet (with the dipole oriented away from the sun); differences in the data pairs, on the average over many Explorer orbits, were considered to represent a measurement of the induced field. At the Explorer 35 periselene the induced field was found to be less than the experimental error. Using the experimental error as the upper limit of the induced field at the surface, Behannon calculated an upper limit of 1.8 for the bulk magnetic permeability of the moon.

2. Results from Simultaneous Apollo and Explorer 35 Measurements. Deployment of Apollo magnetometers on the lunar surface allowed simultaneous measurements of the external inducing field (by Explorer

35) and the total response field at the lunar surface (by an Apollo magnetometer). The total response field measured at the surface by an Apollo magnetometer is the sum of the external and induced fields:

$$\underline{B} = \mu \underline{H} = \underline{H} + 4\pi \underline{M} \qquad (1)$$

where $\underline{H}$ is the external magnetizing field and $\underline{M}$ is the magnetization field induced in the permeable lunar material (see Figure 16). The relative magnetic permeability is $\mu = 1 + 4\pi k$, where k is magnetic susceptibility in emu/cm^3. Since the dipolar magnetization $\underline{M}$ is known to be below the Explorer 35 magnetometer resolution (Behannon, 1968), it is assumed in the dual magnetometer analysis that Explorer 35 measures $\underline{H}$ alone.

For the two-layer lunar permeability model illustrated in Figure 16 (which will be referred to later when iron abundance results are reviewed), the total field at the outer surface of the sphere is expressed

$$\underline{B} = H_x(1 + 2G)\,\hat{x} + H_y(1-G)\,\hat{y} + H_z(1-G)\,\hat{z} \qquad (2)$$

where

$$G = \frac{(2\eta+1)(\mu_1-1) - \lambda^3(\eta-1)(2\mu_1+1)}{(2\eta+1)(\mu_1+2) - 2\lambda^3(\eta-1)(\mu_1-1)} \qquad (3)$$

Here $\eta = \mu_1/\mu_2$; μ_1 and μ_2 are relative permeability of the shell and core, respectively. The permeability exterior to the sphere is $\mu_o = 1$, that of free space; $\lambda = R_c/R_m$; R_c and R_m are radius of the core and the moon, respectively. Equation (2) expresses the total

surface field in a coordinate system which has its origin on the lunar surface at an Apollo magnetometer site: $\hat{x}$ is directed radially outward from the lunar surface, and $\hat{y}$ and $\hat{z}$ are tangential to the surface, directed eastward and northward, respectively.

A plot of any component of equation (2) will result in a B - H hysteresis curve. Equation (3) relates the slope of the hysteresis curve to the lunar permeability. The average whole-moon permeability μ is calculated from the hysteresis-curve slope by setting $\mu_1 = \mu_2 = \mu$ in equation (3):

$$G = \frac{\mu - 1}{\mu + 2} \qquad (4)$$

The hysteresis-curve method of permeability analysis was first employed by Dyal and Parkin (1971) to calculate the whole-moon permeability result 1.03 ± 0.13. Since then the error limits have been lowered by processing a larger number of simultaneous data sets and using more rigid data selection criteria (e.g., Parkin et al., 1973).

In the most recent dual-magnetometer results (Parkin et al., 1974a,b), a hysteresis curve was constructed using 2703 data sets (see Figure 17). Since the external magnetizing field is so small ($\sim$ 10 gammas), the familiar "S" shape of the hysteresis curve degenerates to a straight line (Ellwood, 1934). The data were fit by a least-

squares technique which yields the slope best-estimate of 1.008 ± 0.004. Using this value with the radial (x) component of equation (2) and equation (4), the whole-moon permeability was calculated to be $\mu = 1.012 \pm 0.006$ (2σ error limits). Both extrema are greater than 1.0, implying that the moon, as a whole, acts as a paramagnetic or weakly ferromagnetic sphere. This result has been used to calculate the iron abundance of the moon as discussed in the next section.

C. T. Russell (private communication) has recently made permeability calculations using data from a single magnetometer, the Apollo 15 subsatellite magnetometer orbiting at an altitude about 100 km above the moon. The results to date indicate that the relative permeability of the entire spherical volume enclosed by the satellite orbit is below 1.0, implying that the layer between the moon and the satellite orbit is diamagnetic. Whether such a layer exists is uncertain at this time; further investigation is required using both magnetic and plasma data.

B. Lunar Iron Abundance

Iron abundance calculations have been presented by various authors, in theoretical treatments based on geochemical and geophysical properties calculated for bodies of planetary size (Urey, 1962; Reynolds and Summers, 1969; Urey and MacDonald, 1971) or on measured compositions of meteorites (Wänke et al., 1973). Recently Parkin et al. (1973, 1974 a, b) used a global lunar per-

meability measurement, determined from magnetic field measurements, to calculate lunar iron abundance for the moon. In their calculations the moon was modeled by a homogeneous paramagnetic rock matrix (olivine and orthopyroxene models were used), in which free metallic iron is uniformly distributed. Pyroxenes and olivines have been reported to be major mineral components of the lunar surface fines and rock samples (Nagata et al., 1971; Zussman, 1972; Weeks, 1972), with combined iron present as the paramagnetic Fe^{2+} ion. The ferromagnetic component of lunar samples is primarily metallic iron which is sometimes alloyed with small amounts of nickel and cobalt (Nagata et al., 1972b; Pierce et al., 1971). This free iron is thought to be native to the moon (because of its low nickel content) rather than meteoritic in origin (Strangway et al., 1973a). Orthopyroxene and olivine models are consistent with geochemical studies (Urey et al., 1971 ; Wood et al., 1970; Ringwood and Essene, 1970; Green et al., 1971) and geophysical studies (Toksöz, 1973).

Since the susceptibility of free iron changes several orders of magnitude at the iron Curie temperature (T_c), Parkin et. al. have used a two-layer model with the core-shell boundary R_c at the Curie isotherm (see Figure 16). For $R > R_c$, $T < T_c$, and for $R \leq R_c$, $T > T_c$. Therefore, for $R > R_c$ any free iron is ferromagnetic while at greater depths where $T > T_c$, the free iron is paramagnetic. The Curie iso-

therm location is determined from the thermal profile used for a particular model. Three thermal models have been used in the calculations. For model profile T_1 the Curie isotherm is spherically symmetric and located at $R_c/R_m = 0.9$. Shell and core temperatures are 600°C and 1400°C, respectively. For the model profile T_2 the shell is 500°C and the core is 1300°C, while the Curie isotherm boundary is at $R_c/R_m = 0.85$. Temperatures are 300°C and 700°C for shell and core of model profile T_3, which has $R_c/R_m = 0.7$. In the outer shell there are both ferromagnetic and paramagnetic contributions to the total magnetic permeability $\mu_1 = 1 + 4\pi k_1$. The susceptibility of the shell is $k_1 = k_{1c} + k_{1a}$, where k_{1a} is "apparent" ferromagnetic susceptibility and k_{1c} is paramagnetic susceptibility. The ferromagnetic component is metallic free iron, assumed to be composed of multidomain, noninteracting grains; the paramagnetic component is Fe^{2+} combined in the orthopyroxene or olivine rock matrix. The measured ferromagnetic susceptibility of the shell material is an apparent value which differs from the intrinsic ferromagnetic susceptibility of the iron because of self-demagnetization of the iron grains and the volume fraction of iron in the shell. For $R < R_c$ the lunar material is paramagnetic only, with susceptibility $k_2 = k_{2c} + k_{2a}$; k_{2c} is the contribution of paramagnetic chemically combined iron and k_{2a} is the apparent susceptibility of free paramagnetic iron above the Curie temperature.

From the magnetic properties of lunar compositional and thermal

models, Parkin et al., (1974a) calculated iron abundances for the moon which were consistent with measured global permeability. Their results are summarized in Table 2. The minimum total iron abundance consistent with the hysteresis curve can be calculated assuming the whole-moon permeability corresponds entirely to ferromagnetic iron in the outer shell where the temperature is below the Curie point. For this case the bulk iron abundance is 0.9 ± 0.5 wt. %. It is noted that the susceptibilities of both olivine and pyroxene are about an order of magnitude too small to account for the measured permeability without some ferromagnetic material present.

C. Considerations of an Iron Core and Iron-Rich Layer

The whole-moon permeability was also used by Parkin et al. (1974a) to investigate the magnetic effects of a hypothetical iron core in the moon. Density and moment of inertia measurements for the moon limit the size of such a core to less than 500 km in radius (Toksöz, 1973). If this hypothetical iron core were entirely paramagnetic and the surrounding core were orthopyroxene of average temperature 1100°C the global permeability would be 1.0003. This value is small compared to the measured permeability of 1.012 ± 0.006, implying that if such a small paramagnetic iron core exists, its magnetization is masked by magnetic material lying nearer to the surface. Therefore the hysteresis measurements can neither con-

firm nor rule out the existence of a small iron core in the moon.

An iron-rich layer in the moon has been considered by several investigators (Wood et al., 1970; Urey et al., 1971; Gast and Giuli, 1972). It is possible that early melting and subsequent differention of the outer several hundred kilometers of the moon may have resulted in the formation of a high-density, iron-rich layer beneath a low-density, iron-depleted crust. Constraints have been placed on an iron-rich layer by Gast and Giuli (1972) using geochemical and geophysical data (for example, measurements of lunar moments of inertia). One set of their models consists of high-density layers between depths of 100 km and 300 km. At a depth of 100 km the allowed layer thickness is 12 km; the thickness increases with increasing depth, to 50 km at 300 km depth. Also presented are a set of layers at 500 km depth. Using exactly the same considerations as were used in the iron abundance calculations Parkin et. al. have calculated whole-moon permeabilities which would be expected from lunar models with these iron-rich layers. The calculations indicate that all iron rich layers allowed by geophysical constraints as outlined by Gast and Giuli, if wholly above the iron Curie temperature, would yield global permeabilities of about 1.00006. As for the case of a small lunar iron core, the magnetization field of such paramagnetic layers would be masked by ferromagnetic materials elsewhere in the moon, and the hysteresis

curve measurements can neither confirm nor rule out these layers. This conclusion would particularly apply to the Gast-Giuli layers at 500 km depths, which are almost certainly paramagnetic. If the iron-rich layers are below the Curie temperature and therefore ferromagnetic, they yield global permeabilities of about 3.5. This is above the upper limit for the measured permeability of 1.012 ± 0.006 and the Gast-Giuli layers can be ruled out if they are cool enough to be ferromagnetic. It is important to realize that the high density layers discussed by Gast and Giuli (1972) can be thought of as limiting cases and that there are innumerable less dense and thinner layers which are allowed by geophysical, geochemical and magnetic constraints.

V. GLOBAL EDDY CURRENT INDUCTION: ELECTRICAL CONDUCTIVITY AND TEMPERATURE

Electrical conductivity and temperature of the moon have been calculated from global eddy current response to changes in the magnetic field external to the moon. When the moon is subjected to a change in the external field, an eddy current field is induced in the moon which opposes the change (see Figures 18 and 19). The induced field responds with a time dependence which is a function of the electrical conductivity distribution in the lunar interior. Simultaneous measurements of the transient driving field (by Explorer 35) and the lunar response field (by an Apollo surface magnetometer) allow calculation of the lunar conductivity. Since conductivity is related to temperature, a temperature profile can be calculated for an assumed compositional model of the lunar interior.

When the moon is in the solar wind, lunar eddy current fields form an induced lunar magnetosphere which is distorted in a complex manner due to flow of solar wind plasma past the moon, as illustrated in Figure 18. The eddy current field is compressed on the dayside of the moon and is swept downstream and confined to the "cavity" on the lunar nightside. Because of the complexity, early analysis included a theory for transient response of a sphere in a vacuum to model lunar response as measured on the lunar nightside (Dyal et al., 1970c; Dyal and Parkin, 1971c; Sill, 1972) and

a harmonic theory of a sphere totally confined by the solar wind to model response as measured on the lunar dayside (Sonett et al., 1971, 1972; Kuckes, 1971; Sill, 1972). Both the transient and the harmonic techniques have subsequently been further developed. Transient analysis has evolved to include effects of cavity confinement on nightside tangential data and to introduce analysis of magnetic step transients measured on the lunar dayside (Dyal and Parkin, 1973; Dyal et al., 1973). Harmonic analysis has been developed with the purposes of eventually developing a dynamic response theory for the case of asymmetric confinement (Schwartz and Schubert, 1973) and of extending the data analysis to lower frequencies and correcting for diamagnetic effects in the solar wind (Kuckes et al., 1974).

Recently time-dependent poloidal response of a sphere in a vacuum has been applied to data measured in the geomagnetic tail where plasma confinement effects are minimized. In this section lunar electrical conductivity from transient-response and harmonic analysis results are reviewed with emphasis on the former technique, and preliminary results of transient response analysis in the geomagnetic tail are presented. Also, representative temperature profiles determined from electrical conductivity analyses are presented and compared with temperatures derived from other analytical techniques.

A. Electrical Conductivity Analysis: Moon in Solar Wind Plasma

1. Lunar Nightside Data Analysis: Transient Response

The lunar electrical conductivity has been investigated by analysis of the lunar response to transients in the solar wind magnetic field. The response, measured by an Apollo magnetometer on the nightside of the moon, is theoretically approximated by the response of a conducting sphere in a vacuum. The theory was developed by extending the work of Smythe (1950) and Wait (1951) for a radially varying lunar conductivity profile (Dyal et al., 1972b). The measured response (illustrated in Figure 20a) is the average poloidal field response (for the radial surface field component) to a normalized fast-ramp decrease in the external field. Error bars are standard deviations of the measured responses. Chosen for the analysis is a ramp input function which falls from unity to zero in 15 seconds, a time characterizing convection of a solar wind discontinuity past the Moon. (For a 400 km/sec solar wind, this time is 10-20 sec, depending on the thickness of the discontinuity and the inclination of its normal to the solar wind velocity.)

For a family of conductivity profiles, all of which monotonically increase with depth in the moon, the theoretical response to a fast ramp is calculated and compared to the measured response. A particular set of these conductivity profiles yield response functions which pass within all data error bars of Figure 20a. These

profiles define the shaded region of Figure 23 and are all consistent with the nightside response data.

2. Lunar Dayside Data Analysis: Transient Response.

Theoretical solutions for an eddy current field totally confined to a sphere of homogeneous conductivity are derived from Maxwell's equations in Dyal et al. (1973). Figure 20b shows averages of normalized rising step transients measured on the lunar dayside in response to increasing step transients in the free-streaming solar wind (error bars are standard deviations). The overshoot maximum is amplified by a factor of 5 over the external input field step change, by solar wind dayside confinement of the surface tangential field components. The data are fit by a lunar conductivity model with a homogeneous core of radius $R_c = 0.9R_m$ and conductivity $\sigma \sim 10^{-3}$ mhos/m. This result is consistent with the nightside conductivity profile illustrated in Figure 23 to depths allowed by the duration of the response data which is shown in Figure 20b.

3. Lunar Dayside Data Analysis: Harmonic Response

The harmonic analysis of the lunar conductivity has been applied to data taken on the lunar dayside. The theoretical modeling is based on the assumption that any global induced field is excluded from the oncoming solar wind by currents induced in the highly conducting solar plasma; it is assumed that in effect the solar wind

completely confines the induced field in the lunar interior and in a thin region above the lunar surface. The confinement current is considered to be a surface current and provides a boundary condition of total confinement by currents around the whole moon, permitting solution of Maxwell's equations at the lunar surface. This spherical confinement case is then applied to magnetometer data measured on the lunar sunlit side. Basic theoretical development of harmonic solutions can be found in several references (Backus and Gilbert, 1967; Parker, 1970; Schubert and Schwartz, 1969; Sill and Blank, 1970; Kuckes, 1971).

Once the poloidal fields have been derived, the analytical technique requires calculating frequency-dependent transfer functions which are defined as follows:

$$A_i(f) = \frac{b_{Ei}(f) + b_{Pi}(f)}{b_{Ei}(f)} \qquad (5)$$

$i = x,y,z$, where the A_i are transfer functions of components of frequency-dependent magnetic fields, expressed in the orthogonal coordinate system with origin on the surface of the moon ($\hat{x}$ is radial and $\hat{y}$ and $\hat{z}$ are tangent to the surface); $b_{Ei}(f)$ is the Fourier transform of the external driving magnetic field; and $b_{Pi}(f)$ is the Fourier transform of the induced global poloidal field.

The harmonic data analysis involves Fourier-analyzing simultaneous data from the Apollo 12 lunar surface magnetometer, taken during lunar daytime, and the lunar orbiting Explorer 35 magnetometer.

Then ratios of the surface data to orbital data are used to calculate a transfer function given by equation (5) .

The form of the transfer function is determined by the internal conductivity distribution in the moon; therefore, a "best fit" conductivity profile can be obtained by numerically fitting the measured and theoretical transfer functions. Figure 23 includes the "best fit" conductivity profile of Sonett et al. (1971) obtained in this manner. The conductivity profile is characterized by a large "spike" of maximum conductivity about 1500 km from the lunar center. Other conductivity profiles have been calculated using the Sonett et al. (1971) transfer function, showing that the spike profile is not unique but that the frontside transfer function can be fitted by simpler two- and three-layer models (Kuckes, 1971; Sill, 1972; Sonett et al., 1972; Reisz et al., 1972; Phillips, 1972).

B. Electrical Conductivity Analysis: Moon in the Geomagnetic Tail

The theoretical models outlined so far have all assumed spherical symmetry to describe lunar eddy current response to changes in the external field. However, analyses to date have used data taken when the moon is immersed in the solar wind plasma with asymmetric confinement of the induced fields. The shortcomings of using spherically symmetric approximations to describe the induced lunar magnetosphere, which is actually asymmetrically confined, have been pointed out in the literature for both the nightside vacuum approxi-

mation (see, e.g., Schubert et al., 1973[a]) and the dayside totally-confined approximation (see, e.g., Dyal and Parkin, 1973). Three dimensional, dynamic asymmetric confinement presents a difficult theoretical problem which has not been solved at the time of this writing. Previous theoretical approximations of the asymmetric problem have included a two-dimensional approximation (Reisz et al., 1972); three-dimensional static theory for a point-dipole source, with substantiating laboratory data (Dyal and Parkin, 1973); a three-dimensional "quasi-static" approach (Schubert et al., 1973[b]); and a three-dimensional dynamic theory for one particular orientation of variations in the external field (Schwartz and Schubert, 1973). In order to circumvent this problem, recent analysis has considered lunar eddy current response during times when the moon is in the geomagnetic tail (see Figure 19), where plasma interaction effects encountered in the solar wind (asymmetric confinement, remanent field compression, plasma diamagnetism, etc.) are minimal.

1. Poloidal Response of a Sphere in a Vacuum: Theory

To describe the response of the lunar sphere to an arbitrary input field in the geomagnetic tail, we define the magnetic vector potential $\underline{A}$ such that $\nabla \times \underline{A} = \underline{B}$ and $\nabla \cdot \underline{A} = 0$. We seek the response to an input $\Delta \underline{B}_E b(t)$, where $b(t) = 0$ for $t < 0$ and $b(t)$ approaches unity as $t \to \infty$. (Since the governing equations are linear, the response to a more general input is readily found by superposition.)

The direction of $\underline{\Delta B}_E$ is taken to be the axis of a spherical coordinate system (r, θ, φ). If the conductivity is spherically symmetric, the transient magnetic field response has no φ component, and hence $\underline{A} = \underline{A}\,\hat{e}_\varphi$ and $\partial/\partial\varphi = 0$. Under these conditions (and neglecting displacement currents) the laws of Faraday, Ampere, and Ohm combine to yield the diffusion equation for the magnetic potential (in MKS units):

$$\nabla^2 \underline{A}\,(r, \theta; t) = \mu\,\sigma\,(r)\,\frac{\partial \underline{A}}{\partial t}\,(r, \theta; t) \qquad (6)$$

We have shown in a previous section on magnetic permeability that we may take $\mu \cong \mu_o$ everywhere. Then, for $t > 0$, the magnetic field must be continuous at the surface, so that $\underline{A}$ and $\frac{\partial}{\partial r}\,\underline{A}$ must always be continuous at $r = R_m$, the radius of the sphere. We also have the boundary condition $\underline{A}\,(0,t) = 0$ and the initial condition $\underline{A}\,(r, \theta; \varphi) = 0$ inside the Moon. Outside of the Moon, where $\sigma = 0$,

$$A = \Delta B_E\,\left(\frac{r}{2}\right)\,b(t)\,\sin\theta + \frac{\Delta B_E}{r^2}\,f(t)\,\sin\theta\,. \qquad (7)$$

The first term on the right is a uniform magnetic field modulated by b(t); the second term is the (as yet unknown) external transient response, which must vanish as $r \to \infty$ and $t \to \infty$. Note that at $r = R_m$, where R_m is normalized to unity,

$$A = \Delta B_E\,\sin\theta\,\left(\frac{b(t)}{2} + f(t)\right) \qquad (8)$$

and

$$\frac{\partial A}{\partial r} = \Delta B_E\,\sin\theta\,\left(\frac{b(t)}{2} - 2f(t)\right)\,. \qquad (9)$$

Therefore, at $r = R_m \cong 1$,

$$\frac{\partial A}{\partial r} = -2A + \frac{3}{2}\left(\Delta B_E \sin\theta\, b(t)\right) . \qquad (10)$$

Since the magnetic field is continuous at $r = R$, this is a boundary condition for the interior problem. Letting $G(r,t) = A/\Delta B_E \sin\theta$ and $\bar{G}(r,s)$ be the Laplace transform of G, equation (6) becomes

$$\frac{1}{r}\left(\frac{\partial^2}{\partial r^2}(r\bar{G}) - \frac{2}{r}\bar{G}\right) = s\mu_o\sigma(r)\bar{G} \qquad (11)$$

for the interior. The boundary conditions are

$$\frac{\partial \bar{G}}{\partial r} = -2\bar{G} + \frac{3}{2}\bar{b}(s) \qquad (12)$$

at $r = R$ and

$$\bar{G} = 0 \qquad (13)$$

at $r = 0$.

For a given $\sigma(r)$ and b(t), this system is numerically integrated to obtain $\bar{G}(r,s)$ in the range $0 \leq r \leq R$. The function $\bar{G}(R,s)$ is then numerically inverse Laplace transformed to find the characteristic transient response function f(t) for the system. The resulting f(t) is compared to the measurements and reiterated with a different function $\sigma(r)$ until the error between the calculated f(t) and the measured f(t) is minimized. The final $\sigma(r)$ is not unique; rather a family of $\sigma(r)$ is generated with the constraint that f(t) match the experimental data.

2. Conductivity Results: Geomagnetic Tail Data Analysis

Figure 21 shows an example of a magnetic transient measured in the geomagnetic tail. The data components are expressed in a coordinate system which has its origin on the lunar surface at the Apollo 12 magnetometer site. The x-component is directed radially outward from the lunar surface, while the y-and z-components are tangent to the surface, directed eastward and northward, respectively. The external driving magnetic field (terrestrial) is measured by Explorer 35, whereas the total response field is measured on the lunar surface by Apollo 12.

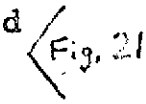

To analyze this and similar events, the Explorer 35 input field components are fitted numerically by functions which are sums of ramp inputs chosen to fit the external field data. For a given conductivity model of the moon, the theoretical time series response to an external field data set is numerically calculated using the theory outlined in the previous section. This calculated response is then compared with the measured Apollo 12 time series data. Conductivity profiles have been constrained to be monotonically increasing with depth into the moon.

Figure 22 shows an example of calculated response for the Explorer 35 x-axis (radial) input function of Figure 21, using the conductivity profile illustrated in Figure 22. Superimposed is the actual response, which is the Apollo 12 x-component of Fig-

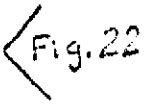

ure 21 . This conductivity profile yields the best fit of 45 profiles which have been run to date, although it is certainly not unique. The profile also yields theoretical responses which fit well for the measured tangential components of Figure 21 and the components of five other geomagnetic tail transients which have been processed to date. The analysis presented here is preliminary; in the future many more transient events will be processed to determine a range of conductivity profiles consistent with a large data set.

In the previous sections various techniques which have been utilized to investigate lunar electrical conductivity were surveyed. Figure 23 shows a summary of conductivity profiles which have been calculated, including profiles based on Fourier-harmonic analysis of dayside lunar data in the solar wind (Sonett et al., 1971; Kuckes et al., 1971); profiles based on transient-response analysis of nightside lunar data in the solar wind (Dyal and Parkin, 1973); and a recent profile from lunar data in the geomagnetic tail.

Fig. 23

C. Lunar Temperature Profiles from Conductivity Analyses

Once the electrical conductivitv profile of the moon has been determined, an internal temperature distribution can be inferred for an assumed lunar material composition (see Rikitake, 1966). For cases where electrical conductivity is independent of pressure

to a first approximation, the conductivity of materials can be expressed in terms of temperature T as follows:

$$\sigma = \sum_i E_i \exp(-a_i/kT) \qquad (14)$$

where a_i are the activation energies of impurity, intrinsic, and ionic modes, expressed in electron volts; E_i are material-dependent constants; and k is Boltzmann's constant. It should be emphasized that the electrical conductivity $\sigma(a, E, T)$ is a strong function of the material composition; therefore uncertainties in knowledge of the exact composition of the sphere limits the accuracy of the internal-temperature calculation.

Laboratory results relating conductivity to temperature for various minerals, which are good geochemical candidates for the lunar interior, have been presented by many investigators (e.g., England et al., 1968; Schwerer et al., 1972; Olhoeft et al., 1973; Duba et al., 1972; Duba and Ringwood, 1973). The recent work by Duba et al. (1972) on the electrical conductivity of olivine ha been used to convert the conductivity profile illustrated in Figure 22 to a temperature profile, shown as number 5 on Figure 24. Also included in this figure are a selection of temperature profiles calculated by other investigators.

VI SUMMARY

A. Lunar Remanent Magnetic Fields

Direct measurements of remanent fields have been made at nine sites on the lunar surface: 38 γ at Apollo 12 in Oceanus Procellarum; 103 γ and 43 γ at two Apollo 14 sites separated by 1.1 km in Fra Mauro; 3 γ at the Apollo 15 Hadley Rille site; and 189 γ, 112 γ, 327 γ, 113 γ, and 235 γ at five Apollo 16 sites in the Descartes region, over a distance of 7.1 km. Simultaneous data from Apollo surface magnetometers and solar wind spectrometers show that the remanent fields at the Apollo 12 and 16 sites are compressed by the solar wind. In response to a solar wind dynamic pressure increase of 1.5×10^{-7} dynes/cm^2, the 38 γ remanent field at the Apollo 12 LSM site is compressed to 54 γ, whereas the field at the Apollo 16 LSM site correspondingly increases from 235 γ to 265 γ. Scale sizes of fields at the Apollo 12 and 16 sites are determined from properties of the remanent field-plasma interaction and orbiting magnetometer measurements. The Apollo 12 scale size L is in the range 2 km $\leq$ L $\leq$ 200 km, whereas for Apollo 16, 5 km $\leq$ L $<$ 100 km.

There is no direct evidence that a global permanent field exists on the moon at present. Analysis of Apollo subsatellite magnetometer data has yielded an upper limit of 4.4×10^{13} gauss-cm^3 for the global permanent field dipole moment.

Measurements by lunar orbiting satellite magnetometers and the

Apollo surface magnetometers, and remanence in the returned samples, have yielded strong evidence that the lunar crustal material is magnetized over much of the lunar globe. Orbiting subsatellite magnetometers have mapped in detail the fields over about 5% of the lunar surface. The maps show that some of the field sources are large-scale, i.e., that subsurface materials may be magnetized in a systematic manner over distances of tens to a few hundreds of kilometers. Furthermore, measured fields tend to be stronger in highland regions than in mare regions, and stronger on the lunar far side than on the near side. The largest magnetic anomaly mapped in detail to date is between the craters Aitken and Van de Graaff on the lunar far side. The origin of lunar remanent field remains an enigma. Possibilities are generally grouped under three classfications: a strong external (solar or terrestrial) field, an ancient intrinsic field of global scale, and smaller localized field sources.

B. Lunar Magnetic Permeability and Iron Abundance

Simultaneous measurements by lunar magnetometers on the surface of the moon and in orbit around the moon are used to construct a whole-moon hysteresis curve, from which the global lunar relative magnetic permeability is determined to be 1.012 ± 0.006. The global induced magnetization dipole moment corresponding to the permeability measurement is $2 \times 10^{22} H$ (where H is magnetizing field in gauss). For typical geomagnetic tail fields of $H \sim 10^{-4}$ gauss, the corresponding

induced dipole moment is 2×10^{18} gauss-cm^3. Both error limits on the magnetic permeability value are greater than 1.0, implying that the moon as a whole is paramagnetic and/or weakly ferromagnetic. Assuming that the ferromagnetic component is free metallic iron of multidomain, noninteracting grains, the free iron abundance in the moon is calculated to be 2.5 ± 2.0 wt. %. Total iron abundance in the moon is determined by combining free iron and paramagnetic iron components for two assumed lunar compositional models. For an orthopyroxene moon of overall density 3.34 g/cm^3 with free iron dispersed uniformly throughout the lunar interior, the total iron abundance is 12.8 ± 1.0 wt. %. For a free iron/olivine moon the total iron abundance is 5.5 ± 1.2 wt. %. A summary of iron abundance calculations is given in Table 2.

Lunar models with a small iron cure and with an iron-rich layer have been investigated using the measured global lunar permeability as a constraint. A small pure iron core of 500 km radius (the maximum size allowed by lunar density and moment of inertia measurements), which is hotter than the iron Curie point ($T>T_c$), would not be resolvable from the data since its magnetization field would be small compared to the measured induced field. Similarly, an iron-rich layer in the moon could not be resolved if the iron is paramagnetic, i.e., if the iron is above the iron Curie temperature. Gast and Giuli (1972) have proposed a family of high-density-layer models for

the moon which are geochemically feasible. If these models are iron-rich layers lying near the lunar surface so that $T<T_c$, the ferromagnetic layers would yield a global permeability value well above the measured upper limit. Therefore it is concluded that such shallow iron-rich-layer models are not consistent with magnetic permeability measurements.

C. Lunar Electrical Conductivity and Temperature

The electrical conductivity of the lunar interior has been investigated by analyzing the induction of global lunar fields by time varying extralunar (solar or terrestrial) magnetic fields. An upper limit on the unipolar induction field has been determined which shows that at least the outer 5 km of the lunar crust is a relatively poor electrical conductor ($< 10^{-9}$ mhos/m) compared to the underlying material. Past conductivity analyses have all used magnetometer data recorded at times when global eddy current fields were asymmetrically confined by the solar wind plasma, using two basic approaches: a time-dependent, transient-response technique and a frequency-dependent, Fourier-harmonic technique. Transient analysis using lunar nightside data yields a conductivity profile rising from about 3×10^{-4} mhos/meter at 170 km depth in the moon to about 10^{-2} mhos/meter at 1000 km depth. Harmonic analyses of dayside data yield profiles generally compatible with nightside transient results only at very shallow depths; deep in the moon the harmonic

results give lower conductivities than do the nightside results.

Recent conductivity analysis has considered lunar eddy current response during times when the moon is in the geomagnetic tail in order to avoid the analytical problems posed by asymmetric solar wind confinement of the induced lunar magnetosphere. Preliminary results show that the following conductivity profile, though not unique, is compatible with input and response data: the conductivity increases rapidly with depth from 10^{-9} mhos/meter at the surface to 10^{-4} mhos/meter at 340 km depth, then less rapidly to 2×10^{-2} mhos/meter at 870 km depth. This conductivity profile is converted to a lunar temperature profile using the data of Duba et. al. (1972) for olivine, and compared to the thermal profile results of other investigators.

Acknowledgments. The authors are grateful to the many individuals who have provided valuable support and encouragement over the past several years, including Dr. T. J. Mucha, K. Lewis, J. Arvin, and R. Marraccini of Computer Science Corporation for programming support; M. Legg, K. Neier and their group at Adia Interim Services for data reduction services; Dr. T. E. Bunch, Dr. P. Cassen, and R. T. Reynolds for theoretical support and technical advice; and J. Keeler, C. Privette, and M. Dix for experiment fabrication and testing. We are pleased to acknowledge research support for C.W.P. under NASA grant no. NGR 05 017 027, and for W.D.D. under NASA grant no. NGR 45 001 040.

REFERENCES

Backus, G.E. and J.F. Gilbert, Numerical applications of a formalism for geophysical inverse problems, Geophys. J. Roy. Astron. Soc., 13, 247-276, 1967.

Barnes, A., P. Cassen, J.D. Mihalov, and A. Eviatar, Permanent lunar surface magnetism and its deflection of the solar wind, Science, 171, 716-718, 1971.

Behannon, K.W., Intrinsic magnetic properties of the lunar body, J. Geophys. Res., 73, 7257, 1968.

Blank, J.L., and W.R. Sill, Response of the moon to the time-varying interplanetary magnetic field, J. Geophys. Res., 74, 736-743, 1969.

Cap, F.F., Possible production mechanisms of lunar magnetic fields, J. Geophys. Res., 77, 3328-3333, 1972.

Clay, D.R., B.E. Goldstein, M. Neugebauer, and C.W. Snyder, Solar-wind spectrometer experiment, in Apollo 15 Preliminary Science Report, NASA SP-289, pp. 10-1 to 10-7, 1972.

Colburn, D.S., R.G. Curie, J.D. Mihalov, and C.P. Sonett, Diamagnetic solar-wind cavity discovered behind the moon, Science, 158, 1040, 1967.

Coleman, P.J., Jr., G. Schubert, C.T. Russell, and L.R. Sharp, The particles and fields subsatellite magnetometer experiment, in Apollo 15 Preliminary Science Report, NASA SP-289, pp. 22-1 to 22-9, 1972a.

Coleman, P.J., Jr., B.R. Lichtenstein, C.T. Russell, G. Schubert, and L.R. Sharp, The particles and fields subsatellite magnetometer

experiment, in Apollo 16 Preliminary Science Report, NASA SP-315, pp. 23-1 to 23-13, 1972b.

Coleman, P.J., Jr., B.R. Lichtenstein, C.T. Russell, L.R. Sharp, and G. Schubert, Magnetic fields near the moon, Proc. Third Lunar Sci. Conf., Geochim. Cosmochim. Acta, Suppl. 3, Vol. 3, edited by D.R. Criswell, pp. 2271-2286, 1972c.

Collinson, D.W., A. Stephenson, and S.K. Runcorn, Magnetic properties of Apollo 15 and 16 rocks, in Proc. Fourth Lunar Sci. Conf. Geochim. Cosmochim. Acta, Suppl. 4, Vol. 3, 2963, MIT Press, 1973.

Criswell, D.R., Photoelectrons and solar wind/lunar limb interaction, The Moon, 7, 202, 1973.

deWys, J.N., Results and implications of magnetic experiments on Surveyor 5, 6, and 7 spacecrafts (abs.), Trans. Am. Geophys. Union, 49, 249, 1968.

Dolginov, Sh. Sh., E.G. Eroshenko, L.N. Zhuzgov, and N.V. Pushkov, Investigation of the magnetic field of the moon, Geomagnetis and Aeronomy, 1, 18, 1961.

Dolginov, Sh. Sh., E.G. Eroshenko, L.N. Zhuzgov, and N.V. Pushkov, Measurements of the magnetic field in the vicinity of the moon by the artificial satellite Luna 10, Akad. Nauk USSR, Doklady, 170, 574, 1966.

Duba, A., and A.E. Ringwood, Electrical conductivity, internal temperatures and thermal evolution of the moon, The Moon, 7, 356, 1973.

Duba, A., H.C. Heard, and R.N. Schock, The lunar temperature profile, Earth Planet. Sci. Letters, 15, 301, 1972.

Dyal, P., and C.W. Parkin, The Apollo 12 magnetometer experiment: Internal lunar properties from transient and steady magnetic field measurements, Proc. Second Lunar Sci. Conf., Geochim. Cosmochim. Acta, Suppl. 2, Vol. 3, 2391, MIT Press, 1971a.

Dyal, P., and C.W. Parkin, The magnetism of the moon, Sci. Amer., 225, 62-73, 1971b.

Dyal, P., and C.W. Parkin, Electrical conductivity and temperature of the lunar interior from magnetic transient-response measurements, J. Geophys. Res., 76, 5947-5969, 1971c.

Dyal, P., and C.W. Parkin, Global electromagnetic induction in the moon and planets, Phys. Earth Plant. Interiors, 7, 251, 1973.

Dyal, P., C.W. Parkin, and C.P. Sonett, Apollo 12 magnetometer: Measurement of a steady magnetic field on the surface of the moon, Science, 169, 762, 1970a.

Dyal, P., C.W. Parkin, and C.P. Sonett, Lunar surface magnetometer, IEEE Trans. on Geoscience Electronics, GE-8(4), 1970b.

Dyal, P., C.W. Parkin, C.P. Sonett, and D.S. Colburn, Electrical conductivity and temperature of the lunar interior from magnetic transient response measurements, NASA TMX-62,012, 1970c.

Dyal, P., C.W. Parkin, C.W. Snyder, and D.R. Clay, Measurements of lunar magnetic field interaction with the solar wind, Nature, 236, 381-385, 1972a.

Dyal, P., C.W. Parkin, and P.Cassen, Surface magnetometer experiments: Internal lunar properties and lunar surface interactions with the solar plasma, Proc. Third Lunar Sci. Conf., Geochim. Cosmochim. Acta, Suppl. 3, Vol. 3, 2287, edited by D.R. Criswell, MIT Press, 1972b.

Dyal, P., C.W. Parkin, C.P. Sonett, R.L. DuBois, and G. Simmons, Lunar portable magnetometer experiment, Apollo 16 Preliminary Science Report, NASA SP-315, pp. 12-1 to 12-8, 1972c.

Dyal, P., C.W. Parkin, and W.D. Daily, Surface magnetometer experiments: Internal lunar properties, Proc. Fourth Lunar Science Conf., Geochim. Cosmochim. Acta, Suppl. 4, edited by W.A. Gose, Vol. 3, pp. 2229-2945, Pergamon, 1973.

Ellwood, W.B., A new ballistic galvanometer operating in high vacuum, Rev. Sci. Inst., 5, 300-305, 1934.

England, A.W., G. Simmons, and D. Strangway, Electrical conductivity of the moon, J. Geophys. Res., 73, 3219, 1968.

Fuller, M., Lunar magnetism, Rev. Geophys. and Space Sci., in press, 1974.

Gast, P.W., and R.T. Giuli, Density of the lunar interior, Earth Planet. Sci. Letters, 16, 299, 1972.

Gold, T., The magnetosphere of the moon, in The Solar Wind, edited by R.J. Mackin, Jr., and M. Neugebauer, Pergamon Press, New York, 1966.

Gopulan, K., S. Kaushal, C. Lee-Hu, and G.W. Wetherill, Rb-Sr and U,

Th-Pb ages of lunar materials, Proc. Apollo 11 Lunar Sci. Conf., Geochim. Cosmochim. Acta, Suppl. 1, Vol. 2, 1195-1205, Pergamon Press, 1970.

Gordon, D.I., R.H. Lundsten, and R.A. Chiarodo, Factors affecting the sensitivity of gamma-level ring-core magnetometers, IEEE Trans. on Magnetics, MAG-1(4), 330, 1965.

Gose, W.A., D.W. Strangway, and G.W. Pearce, A determination of the intensity of the ancient lunar magnetic field, The Moon, 5, 1972.

Green, D.H., A.E. Ringwood, N.G. Ware, W.O. Hibberson, A. Major, and E. Kiss, Experimental petrology and petrogenesis of Apollo 12 basalts, Proc. Second Lunar Sci. Conf., Geochim. Cosmochim. Acta, Suppl. 2, Vol. 1, edited by A.A. Levinson, MIT Press, 601-615, 1971.

Hinners, N.W., The new moon: A view, Rev. Geophys. and Space Phys., 9, 447, 1971.

Helsley, C.E., Magnetic properties of lunar 10022, 10069, 10084, and 10085 samples, Proc. Apollo 11 Lunar Sci. Conf., Geochim. Cosmochim. Acta, Suppl. 1, Vol. 3, 2213, Pergamon, 1970.

Hobbs, B.A., The inverse problem of the moon's electrical conductivity, Earth Planet. Sci. Letters, 17, 380-384, 1973.

Kuckes, A.F., Lunar electrical conductivity profile, Nature, 232, 249, 1971.

Kuckes, A.F., W.D. Daily, P. Dyal, and C.W. Parkin, Temperature profile of the lunar interior (abs.), submitted to Trans. Amer.

Geophys. Union (EOS), Vol. 55, 1974.

Levy, E.H., Magnetic dynamo in the moon: A comparison with earth, Science, 178, 52, 1972.

Michel, F.C., Magnetic field structure behind the moon, J. Geophys. Res., 73, 1533, 1968.

Mihalov, J.D., D.S. Colburn, R.G. Currie, and C.P. Sonett, Configuration and reconnection of the geomagnetic tail, J. Geophys. Res. 73, 943, 1968.

Mihalov, J.D., C.P. Sonett, J.H. Binsack, and M.D. Moutsoulas, Possible fossil lunar magnetism inferred from satellite data, Science, 171, 892, 1971.

Murthy, V.R. and S.K. Banerjee, Lunar evolution: How well do we know it now, The Moon, 7, 149, 1973.

Nagata, T., Y. Ishikawa, H. Kinoshita, M. Kono, Y. Syono, and R.M. Fisher, Magnetic properties and natural remanent magnetization of lunar materials, Proc. of the Apollo 11 Lunar Science Conf. Geochim. Cosmochim. Acta, suppl. 1, Vol. 3, 2325, Pergamon Press, 1970.

Nagata, T., R.M. Fisher, F.C. Schwerer, M.D. Fuller, and J.R. Dunn, Magnetic properties and remanent magnetization of Apollo 12 lunar materials and Apollo 11 lunar microbreccia, Proc. Second Lunar Sci. Conf., Geochim. Cosmochim. Acta, suppl. 2, Vol. 3, 2461, MIT Press, 1971.

Nagata, T., R.M. Fisher, and F.C. Schwerer, Lunar rock magnetism, The Moon, 4, 1972a.

Nagata, T., R.M. Fisher, F.C. Schwerer, M.D. Fuller, and J.R. Dunn, Rock magnetism of Apollo 14 and 15 materials. Proc. Third Lunar Sci. Conf. Geochim. Cosmochim. Acta, suppl. 3, Vol. 3, 2423, MIT Press, 1972b.

Ness, N.F., Electrical conductivity of the moon (abs.), Trans. Am. Geophys. Union, 49, 242, 1968.

Ness, N.F., K.W. Behannon, C.S. Scearce, and S.C. Cantarano, Early results from the magnetic field experiment on Explorer 35, J. Geophys. Res., 72, 5769, 1967.

Olhoeft, G.R., A.L. Frisillo, D.W. Strangway, and H. Sharpe, Electrical properties of lunar solid samples, in Lunar Science IV, edited by J. Chamberlain and C. Watkins, The Lunar Science Institute, Houston, pp. 575-577, 1973.

Parker, R.L., The inverse problem of electrical conductivity in the mantle, Geophys. J. Roy. Astron. Soc., 22, 121-138, 1970.

Parkin, C.W., P. Dyal and W.D. Daily, Iron abundance in the moon from magnetometer measurements, Proc. Fourth Lunar Sci. Conf., Geochim. Cosmochim. Acta, suppl. 4, Vol. 3, 2947, Pergamon Press, 1973.

Parkin, C.W., W.D. Daily and P. Dyal, Iron abundance in the moon, submitted to Ap. J., 1974a.

Parkin, C.W., W.D. Daily, and P. Dyal, Lunar iron abundance from magnetometer measurements, in Lunar Science V, Part II, p. 589, The Lunar Science Institute, Houston, 1974b.

Pearce, G.W., D.W. Strangway, and E.E. Larson, Magnetism of two Apollo 12 igneous rocks, Proc. Second Lunar Sci. Conf., Geochim. Cosmochim. Acta, suppl. 2, Vol. 3, 2451, MIT Press, 1971.

Pearce, G.W., W.A. Gose, and D.W. Strangway, Magnetic studies on Apollo 15 and 16 lunar samples, Proc. Fourth Lunar Sci. Conf., Geochim. Cosmochim. Acta, Suppl. 4, Vol. 3, Pergamon Press, 3045 - 3076, 1973.

Phillips, R.J., The lunar conductivity profile and the nonuniqueness of electromagnetic data inversion, Icarus, 17, 88-103, 1972.

Reisz, A.C., D.L. Paul, and T.R. Madden, The effects of boundary condition asymmetries on the interplanetary magnetic field-moon interaction, The Moon, 4, 134-140, 1972.

Reynolds, R.T., and A.L. Summers, Calculations on the composition of the terrestrial planets, J. Geophys. Res., 74, 2494, 1969.

Rikitake, T., Electromagnetism and the Earth's Interior, Elsevier, Amsterdam, 1966.

Ringwood, A.E., and E. Essene, Petrogenesis of lunar basalts and the internal constitution and origin of the moon, Science, 167, 607 - 610, 1970.

Runcorn, S.K., D.W. Collinson, W. O'Reilly, M.H. Battey, A.A. Stephenson, J.M. Jones, A.J. Manson, and P.W. Readman, Magnetic properties of Apollo 11 lunar samples, in Proc. of the Apollo 11 Lunar Sci. Conf., Geochim. Cosmochim. Acta, Suppl. 1, Vol. 3, edited by A.A. Levinson, Pergamon Press, New York, p. 2369, 1970.

Runcorn, S.K., D.W. Collinson, W. O'Reilly, A. Stephenson, M.H. Battey, A.J. Manson, and P.W. Readman, Magnetic properties of Apollo 12 lunar samples, Proc. Roy. Soc. London, Ser. A, 325, 157, 1971.

Russell, C.T., P.J. Coleman, Jr., B.R. Lichtenstein, G. Schubert, and L.R. Sharp, Subsatellite measurements of the lunar magnetic field, Proc. Fourth Lunar Sci. Conf., Geochim. Cosmochim. Acta, Suppl. 4, edited by W.A. Gose, Vol. 3, pp. 2833-2845, 1973.

Schubert, G., and K. Schwartz, A theory for the interpretation of lunar surface magnetometer data, The Moon, 1, 106, 1969.

Schubert, G., B.F. Smith, C.P. Sonett, D.S. Colburn., and K. Schwartz, The night side electromagnetic response of the moon, J. Geophys. Res., 78, 3688-3696, 1973a.

Schubert, G., C.P. Sonett, K. Schwartz, and H.J. Lee, Induced magnetosphere of the moon 1. Theory, J. Geophys. Res., 78, 2094-2110, 1973b.

Schubert, G., K. Schwartz, C.P. Sonett, D.S. Colburn, and B.F. Smith, Lunar electromagnetic Scattering II. Magnetic fields and transfer functions for parallel propagation, Proc. Fourth Lunar Sci. Conf., Geochim. Cosmochim. Acta., Suppl. 4, edited by W.A. Gose, Vol. 3, pp. 2909-2923, Pergamon, 1973c.

Schubert, G., B.F. Smith, C.P. Sonett, D.S. Colburn, and K. Schwartz, Polarized magnetic field fluctuations at the site of Apollo 15: Possible regional influence on lunar induction, submitted to Science, 1974.

Schwartz, K., and G. Schubert, Time-dependent lunar electric and magnetic fields induced by a spatially varying interplanetary magnetic field, J. Geophys. Res., 74, 4777-4780, 1969.

Schwartz, K., and G. Schubert, Lunar electromagnetic scattering I. Propagation parallel to the diamagnetic cavity axis, J. Geophys. Res., 78, 6496-6506, 1973.

Schwartz, K., C.P. Sonett, and D.S. Colburn, Unipolar induction in the moon and a lunar limb shock mechanism, The Moon, 1, 7, 1969.

Schwerer, F.C., G.P. Huffman, R.M. Fisher, and T. Nagata, D.C. electrical conductivity of lunar surface rocks, The Moon, 4, 187, 1972.

Sharp, L.R., P.J. Coleman, Jr., B.R. Lichtenstein, C.T. Russell, G. Schubert, Orbital mapping of the lunar magnetic field, The Moon, 7, 322, 1973.

Sill, W.R., Lunar conductivity models from the Apollo 12 magnetometer experiment, The Moon, 4, 3-17, 1972.

Sill, W.R., and J.L. Blank, Method for estimating the electrical conductivity of the lunar interior, J. Geophys. Res., 75, 201, 1970.

Smith, B.F., D.S. Colburn, G. Schubert, K. Schwartz, and C.P. Sonett, Induced magnetosphere of the moon 2. Experimental results from Apollo 12 and Explorer 35, J. Geophys. Res., 78, 5437-5448, 1973.

Smolychowski, R., Magnetism of the moon, The Moon, 7, 127, 1973.

Smythe, W.R., Static and Dynamic Electricity, McGraw-Hill Book Co., New York, 1950.

Sonett, C.P., and D.S. Colburn, Establishment of a lunar unipolar generator and associated shock and wake by the solar wind, Nature, 216, 340, 1967a.

Sonett, C.P., D.S. Colburn, and R.G. Currie, The intrinsic magnetic field of the moon, J. Geophys. Res., 72, 5503, 1967a.

Sonett, C.P., D.S. Colburn, R.G. Currie, and J.D. Mihalov, The geomagnetic tail: topology, reconnection and interaction with the moon, in Physics of the Magnetosphere, edited by R.L. Carovillano, J.F. McClay, and H.R. Radoski, D. Reidel Publishing Co., Dordrecht, Holland, 1967b.

Sonett, C.P., D.S. Colburn, P. Dyal, C.W. Parkin, B.F. Smith, G. Schubert, and K. Schwartz, Lunar electrical conductivity profile, Nature, 230, 359, 1971.

Sonett, C.P., B.F. Smith, D.S. Colburn, G. Schubert, and K. Schwartz, The induced magnetic field of the moon: conductivity profiles and inferred temperature, Proc. Third Lunar Sci. Conf., Geochim. Cosmochim. Acta, Suppl. 3, Vol. 3, The MIT Press, p. 2309, 1972.

Spreiter, J.R., M.C. Marsh, and A.L. Summers, Hydromagnetic aspects of solar wind flow past the moon, Cosmic Electrodynamics, 1, 5, 1970.

Strangway, D.W., E.E. Larson, and G.W. Pearce, Magnetic studies of lunar samples - breccia and fines, in Proc. Apollo 11 Lunar Sci. Conf., Geochim. Cosmochim. Acta, Suppl. 1, Vol. 3, edited by A.A. Levinson, Pergamon Press, New York, p. 2435, 1970.

Strangway, D.W., G.W. Pearce, W.A. Gose, and R.W. Timme, Remanent magnetization of lunar samples, Earth Planet. Sci. Lett., 13, 43, 1971.

Strangway, D.W., W.A. Gose, G.W. Pearce, and J.G. Carnes, Magnetism and the history of the moon, Proc. of the 18th Annual Conf. on Magnetism and Magnetic Materials, J. Applied Phys., in press, 1973a.

Strangway, D.W., W.A. Gose, G.W. Pearce, and R.K. McConnell, Lunar magnetic anomalies and the Cayley formation, Nature, 246, 112, 1973b.

Strangway, D.W., H.N. Sharp, W. Gose, and G.W. Pearce, Magnetism and the early history of the moon, Geochim. Cosmochim. Acta, 37, Suppl. 4, in press, 1973c.

Toksöz, M.N., preprint, 1973.

Tozer, D.C., and J. Wilson, III, The electrical conductivity of the moon, the electrical conductivity of the moon's interior, Proc. Roy. Soc. London, A296, 320, 1967.

Urey, H.C., The Moon, ed. Z. Kopal and Z.K. Mikhailov, p. 133, Academic Press, 1962.

Urey, H.C. and G.J.F. MacDonald, Origin and history of the moon, in Physics and Astronomy of the Moon, edited by Z. Kopal, p. 213, Academic Press, 1971.

Urey, H. and S.K. Runcorn, A new theory of lunar magnetism, Science, 180, 636, 1973.

Urey, H.C., K. Marti, J.W. Hankins, and M.K. Liu, Model history of the lunar surface, Proc. Second Lunar Sci. Conf., Geochim. Cosmochim. Acta, Suppl. 2, Vol. 3, p. 987, MIT Press, 1971.

Wait, J.R., A conducting sphere in a time varying magnetic field, Geophysics, 16, 666, 1951.

Wänke, H., H. Baddenhausen, G. Dreibus, M. Quijano-Rico, M. Palme, B. Spettel, and F. Teschke, Multielement analysis of Apollo 16 samples and about the composition of the whole moon, in Lunar Science IV, editors J.W. Chamberlain and C. Watkins, pp. 761-763, Lunar Science Institute, Houston, 1973.

Weeks, R.A., Magnetic phases in lunar material and their electron magnetic resonance spectra: Apollo 14., Proc. Third Lunar Sci. Conf., Geochim. Cosmochim. Acta, Suppl. 3, Vol. 3, 2503, MIT Press, 1972.

Wood, J.A., J.S. Dickey, U.B. Marvin, and B.J. Powell, Proc. Apollo 11 Lunar Sci. Conf., Geochim. Cosmochim. Acta, Suppl. 1, Vol. 1, 965, Pergamon Press, 1970.

Zussman, J., The minerology, petrology and geochemistry of lunar samples - a review, The Moon, 5, 422, 1972.

Table 1. Summary of Lunar Surface Remanent Magnetic Field Measurements.
(From Dyal et al., 1973)

Site	Coordinates, deg.	Field Magnitude, Gammas	Magnetic-field components, gammas		
			Up	East	North
Apollo 16:					
ALSEP Site	8.9°S, 15.5°E	235 ± 4	-186 ± 4	-48 ± 3	+135 ± 3
Site 2		189 ± 5	-189 ± 5	+3 ± 6	+10 ± 3
Site 5		112 ± 5	+104 ± 5	-5 ± 4	-40 ± 3
Site 13		327 ± 7	-159 ± 6	-190 ± 8	-214 ± 6
LRV Final Site		113 ± 4	-66 ± 4	-76 ± 4	+52 ± 2
Apollo 15:					
ALSEP Site	26.1°N, 3.7°E	3.4 ± 2.9	+3.3 ± 1.5	+0.9 ± 2.0	-0.2 ± 1.5
Apollo 14:	3.7°S, 17.5°W				
Site A		103 ± 5	-93 ± 4	+38 ± 5	-24 ± 5
Site C′		43 ± 6	-15 ± 4	-36 ± 5	-19 ± 8
Apollo 12:					
ALSEP Site	3.2°S, 23.4°W	38 ± 2	-25.8 ± 1.0	+11.9 ± 0.9	-25.8 ± 0.4

TABLE 2. IRON ABUNDANCE OF THE MOON AS A FUNCTION OF THERMAL AND COMPOSITIONAL MODELS

(From Parkin et al., 1974a)

	Free Iron Abundance, wt. %			Total Iron Abundance, wt. %		
thermal model / compositional model	T_3	T_2	T_1	T_3	T_2	T_1
orthopyroxene	1.0 ± 0.5	2.0 ± 1.0	3.0 ± 1.5	13.4 ± 0.3	13.0 ± 0.5	12.6 ± 0.6
olivine	1.0 ± 0.5	2.0 ± 1.0	3.0 ± 1.5	6.5 ± 0.3	5.9 ± 0.7	5.3 ± 1.0

Free iron abundance:

2.5 ± 2.0 wt. %

Total iron abundance:

9.0 ± 4.7 wt. %

FIGURE CAPTIONS

Fig. 1. Locations of lunar magnetometer experiments. The U.S.S.R. Luna 2 spacecraft, which impacted the moon in 1961, and the Luna 10 orbiter, launched in 1966, made the earliest magnetic measurements in the lunar environment but were not sensitive enough to detect either the permanent or the transient lunar fields. The U.S. Explorer 35 magnetometers, placed in lunar orbit in 1967, made possible the detailed study of the moon's interaction with the solar wind. Permanent and induced lunar fields were first measured by the Apollo surface magnetometers (deployed during four missions from 1969 to 1972); the data have been analyzed to determine properties of the lunar interior. Two Apollo subsatellite magnetometers, close-orbited in 1971 and 1972, have provided detailed magnetic maps over portions of the moon's surface.

Fig. 2. The Apollo 12 lunar surface magnetometer (LSM), deployed in Oceanus Procellarum. Similar instruments were also deployed at the Apollo 15 site near Hadley Rille and the Apollo 16 Descartes site.

Fig. 3. Apollo lunar magnetometers. (a) The Apollo 15 subsatellite magnetometer, orbited at an altitude of approximately 100 kilometers above the lunar surface. A similar satellite was orbited during the Apollo 16 mission. (b) The Apollo 16 lunar portable magnetometer (LPM), carried aboard the lunar roving

vehicle (foreground) and deployed at four locations of the astronaut traverse. A similar instrument was deployed at the Apollo 14 Fra Mauro site.

Fig. 4. Magnetic environment of the moon during a lunar orbit, with emphasis on the geomagnetic tail region. The plane of the lunar orbit very nearly coincides with the ecliptic plane of the earth's orbit. The earth's permanent dipole field is swept back into a cylindrical region known as the geomagnetic tail; at the lunar distance the field magnitude is $\sim$10 gammas (10^{-4} gauss). Substructure of the tail includes two lobes which are separated by the neutral sheet current boundary; the upper or northward lobe has its magnetic field pointing roughly toward the earth, whereas the southward lobe field points away from the earth. The moon is immersed in the tail about four days of each orbit; the moon can pass through either or both lobes.

Fig. 5. Lunar remanent magnetic field measured at the Apollo 12 site in Oceanus Procellarum. (a) Lunar Orbiter photograph showing the Apollo 12 landing site and location of the surface magnetometer where the remanent field measurement was made. (b) Magnitude and orientation of the measured vector magnetic field.

Fig. 6. Lunar remanent magnetic fields measured at the Apollo 14 site at Fra Mauro. (a) Lunar Orbiter photograph showing the Apollo 14 landing site and the locations of sites A and C′ where the lunar portable magnetometer measurements were made. (b) Magnitude and orientation of the measured remanent magnetic fields.

Fig. 7. Lunar remanent magnetic field measured at the Apollo 15 site near Hadley Rille. (a) Photograph showing the Apollo 15 landing site and location of the surface magnetometer where the remanent field measurement was made. (b) Magnitude and orientation of the measured remanent magnetic field.

Fig. 8. Lunar remanent magnetic fields measured at the surface Apollo 16 Descartes site. (a) Photograph showing the Apollo 16 landing site, the location of the surface magnetometer, and the traverse positions where the portable magnetometer was deployed. (b) Magnitude and orientation of the measured vector remanent magnetic fields.

Fig. 9. Magnetic energy density versus plasma energy density at two Apollo sites which have different remanent magnetic fields. The magnetic energy density is computed from the difference between the compressed and uncompressed remanent field at the Apollo sites. Plasma energy density data are calculated from Apollo solar wind spectrometer (SWS) measurements. N is the proton number density, m is the proton mass, and v is the

plasma bulk speed. Apollo 12 magnetometer data are plotted versus Apollo 12 solar wind spectrometer data, while Apollo 16 magnetometer data are plotted versus Apollo 15 SWS data. SWS data are courtesy of C. W. Snyder and D. R. Clay of the Jet Propulsion Laboratory. Uncompressed remanent field magnitudes are 38 γ at Apollo 12 and 235 γ at Apollo 16 LSM sites. (From Dyal et al., 1973.)

Fig. 10. Contour map of the radial component of the lunar remanent magnetic field measured by the Apollo 15 subsatellite magnetometer. Contour labels are in hundredths of gammas, and positive values indicate fields directed out from the surface. This map shows the eastern half of the lunar far side. (From Sharp et al., 1973.)

Fig. 11. Contour map of the radial component of the lunar remanent magnetic field measured by the Apollo 15 subsatellite magnetometer. Contour labels are in hundredths of gammas and positive values indicate fields directed out from the surface. This map shows the western half of the lunar far side. (From Sharp et al., 1973).

Fig. 12. Contour map of the radial component of the lunar remanent magnetic field measured by the Apollo 15 subsatellite magnetometer. Contour labels are in hundredths of gammas and positive values indicate fields directed out from the surface. This map shows the eastern half of the lunar near side

(From Sharp et al., 1973).

Fig. 13. Contour map of the radial component of the lunar remanent magnetic field measured by the Apollo 15 subsatellite magnetometer. Contour labels are in hundredths of gammas and positive values indicate fields directed out from the surface. This map shows the western half of the lunar near side (From Sharp et al., 1973).

Fig. 14. Schematic representation of some global mechanisms proposed to explain the origin of lunar remanent magnetic fields. (a) Large solar or terrestrial field (b) ancient magnetized core (c) iron core dynamo. Description of the mechanisms are given in the text.

Fig. 15. Schematic representation of some local mechanisms proposed to explain the origin of lunar remanent magnetic fields. (a) Shallow Fe - FeS Dynamo (b) Local induced unipolar dynamo (c) Local Thermoelectric dynamo (d) Shock magnetization. Descriptions of the mechanisms are given in the text.

Fig. 16. Magnetization induction in the moon. When the moon is immersed in a uniform external field $\underline{H}$ (in this case the steady geomagnetic tail field), a dipolar magnetization field $\underline{M}$ is induced in permeable material in the lunar interior, with the dipole axis of $\underline{M}$ aligned along the direction of $\underline{H}$. The total magnetic field near the moon is $\underline{B} = \underline{H} + 4\pi\underline{M}$. The magnetic permeabilities of the two layers are μ_1 and μ_2, and

for regions outside the moon, $\mu = \mu_o = 1$ (free space). $\underline{H}$ is measured by the lunar orbiting Explorer 35, whereas $\underline{B}$ is measured by an Apollo lunar surface magnetometer (LSM). Measurements of $\underline{B}$ and $\underline{H}$ allow construction of a B-H hysteresis curve for the sphere, from which permeability and iron abundance can be calculated (From Parkin et al., 1973).

Fig. 17. Hysteresis curve for the moon. Data points are 2703 simultaneous 2-minute averages of radial components of the external geomagnetic field data $\underline{H}$ (measured by the lunar orbiting Explorer 35 Ames magnetometer) and total magnetic induction $\underline{B} = \mu\underline{H}$ ($\underline{B}$ is measured by the Apollo 12 lunar surface magnetometer). Data points are selected from four lunations of measurements made when the moon was immersed in the uniform geomagnetic tail field. In this low-external-field regime ($\sim$10 gammas or 10^{-4} Oe), the hysteresis curve is linear and is fitted by a least-squares line of slope 1.008 $\pm$ 0.004. This slope corresponds to a whole-moon magnetic permeability of 1.012 $\pm$ 0.006 (From Parkin et al., 1974a).

Fig. 18. Global eddy current induction: Moon in the solar wind. Eddy currents and corresponding poloidal magnetic fields are induced by response to time-dependent fluctions in the external field $\underline{B}_E$. The poloidal field has different characteristics, depending on the moon's environment. When the moon is in the solar wind, the global induced field is asymmetri-

cally confined by the solar wind flowing past the moon; the field is compressed on the day (sunlit) side and confined in the cavity region on the night (antisolar) side of the moon.

Fig. 19. Global eddy current induction: Moon in the geomagnetic tail. The induced poloidal field experiences greatly reduced plasma effects, especially in deep-lobe regions of the tail far from the neutral sheet. The poloidal field can be considered to be an unconfined (vacuum) dipole field for analytical purposes.

Fig. 20. Transient response data, measured when moon was in the solar wind. (a) Nightside transient response data, showing decay characteristics of the radial component of the total surface field B_{Ax} after arrival of a step transient which reduces the external magnetic field radial component by an amount ΔB_{Ex}, here normalized to one. The shape of the curve illustrates time characteristics of the decay of the induced poloidal eddy-current field (from Dyal and Parkin, 1973). (b) Daytime transient response data, showing decay characterestics of tangential components ($B_{Ay,z}$) of the total surface field after arrival of a step transient which increases the external magnetic field tangential component by an amount $\Delta B_{Ey,z}$, here normalized to one. Shape of the curve again illustrates decay characteristics of the induced poloidal field. The overshoot maximum is amplified to ~ 5 by solar wind

dayside compression; the theoretical overshoot maximum is 1.5 for an unconfined poloidal field (from Dyal et al., 1973).

Fig. 21. Transient event in the geomagnetic tail, measured simultaneously by the Apollo 12 LSM and the Explorer 35 Ames magnetometer. Data are expressed in the surface coordinate system which has its origin at the Apollo 12 magnetometer site; $\hat{x}$ is directed radially outward from the surface, while $\hat{y}$ and $\hat{z}$ are tangent to the surface, directed eastward and northward, respectively. Due to poloidal field induction in the moon, the Apollo 12 radial ($\hat{x}$) component is "damped" relative to the Explorer 35 radial component, whereas the Apollo 12 tangential ($\hat{y}$ and $\hat{z}$) field components are "amplified" relative to Explorer 35 data. Apollo 12 and Explorer 35 component data scales differ due to the existence of a 38 ± 3 gamma remanent field at the Apollo 12 surface site.

Fig. 22. Electrical conductivity analysis for a transient event in the geomagnetic tail. Shown are data from the radial component of the event of Figure 21. Response to the Explorer 35 external field radial component is computed numerically for the conductivity profile shown in the insert and compared to the measured Apollo 12 response field. In the preliminary results of geomagnetic tail conductivity analysis, this selected conductivity profile, though not unique, yields a satisfactory

fit of input and response data for this and five other tail events processed to date.

Fig. 23. Electrical conductivity profiles calculated for the moon by different techniques and investigators. (1) Geomagnetic tail transient analysis of the data shown in Figures 21 and 22. (2) Nightside transient analysis in the solar wind (Dyal and Parkin, 1973). (3) Dayside harmonic analysis in the solar wind (Sonett et al., 1971) and (4) Kuckes, (1971).

Fig. 24. Temperature profiles calculated by different investigators. (1) Urey (1962). (2) Fricker et al. (1967). (3) Hanks and Anderson (1972). (4) Toksöz and Solomon (1973). (5) Temperature profile calculated from the conductivity profile shown in Figure 22 insert, using the laboratory data for olivine from Duba et al. (1972).

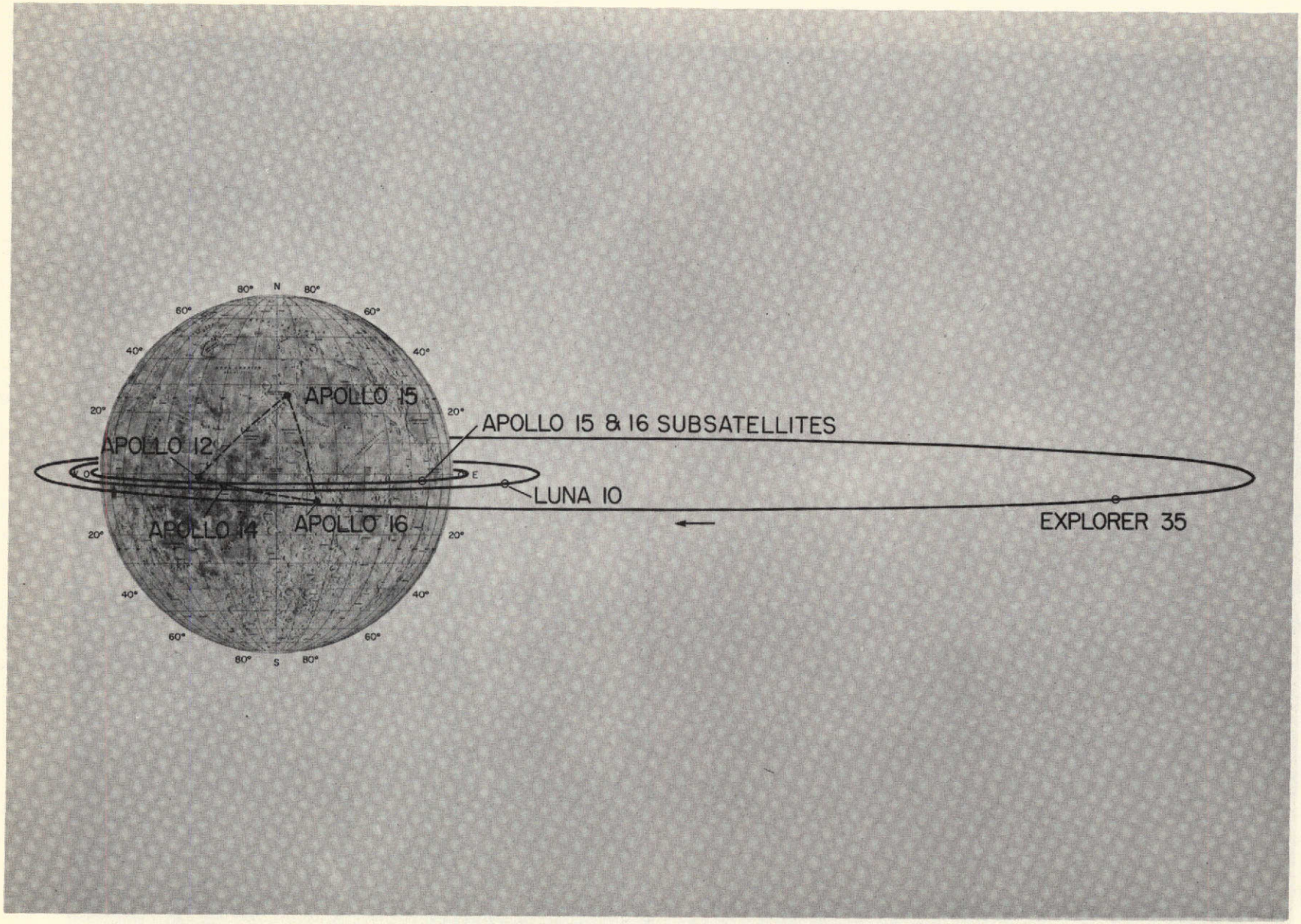
80° N 80°
60° 60°
40° 40°
20° 20°
APOLLO 15
APOLLO 12
APOLLO 14
APOLLO 16
APOLLO 15 & 16 SUBSATELLITES
LUNA 10
EXPLORER 35
20° 20°
40° 40°
60° 60°
80° S 80°

Fig. 1

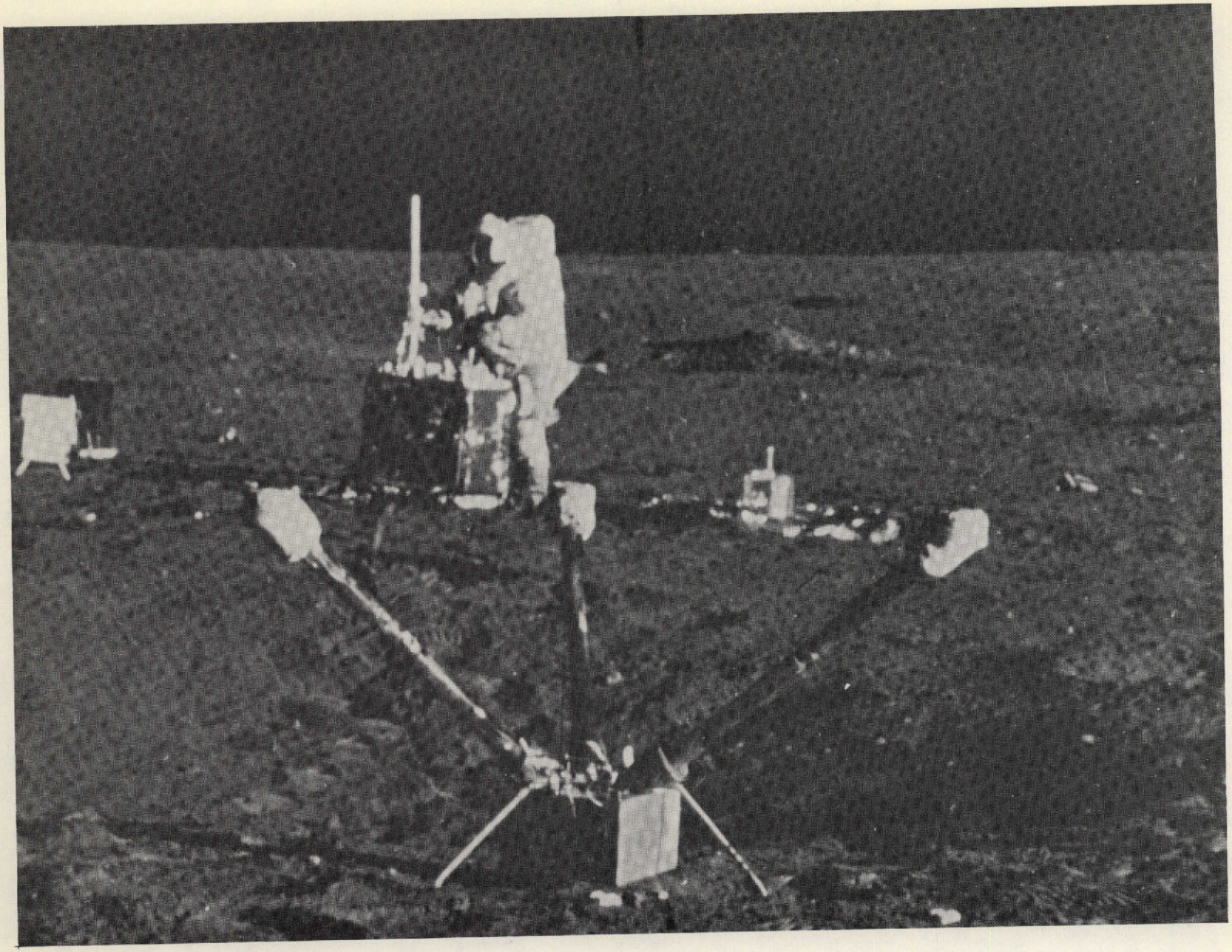

Fig. 2

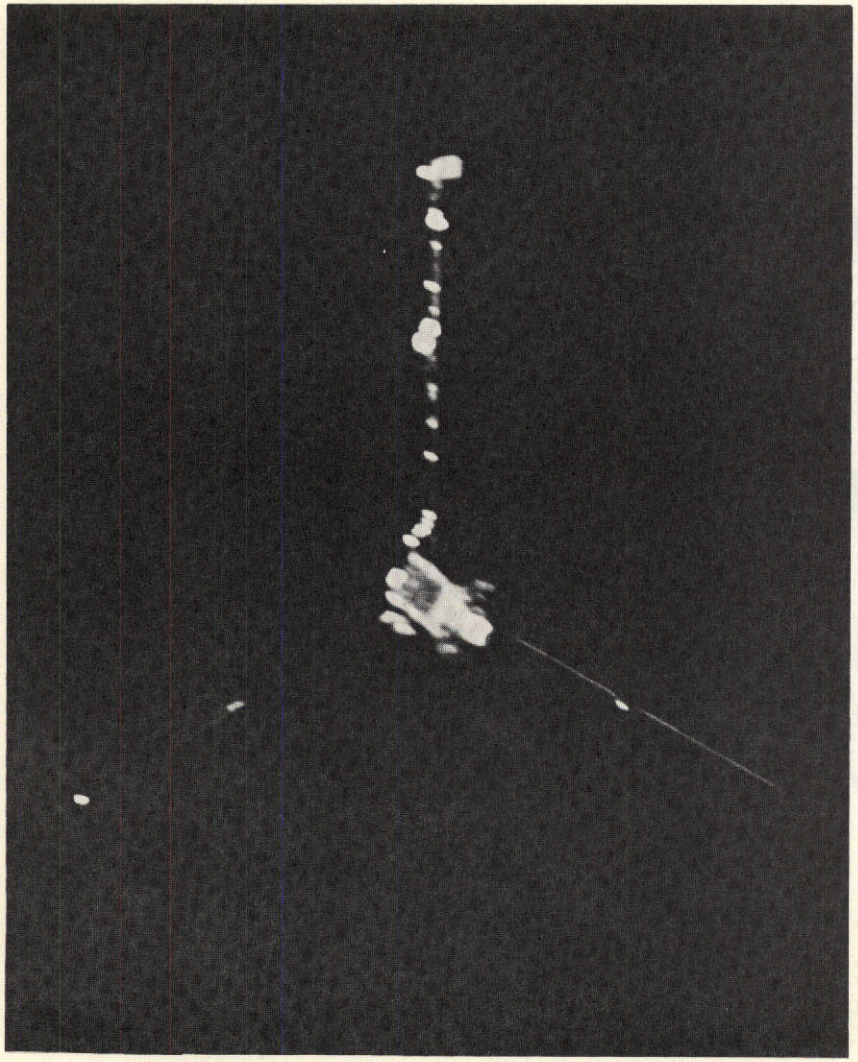

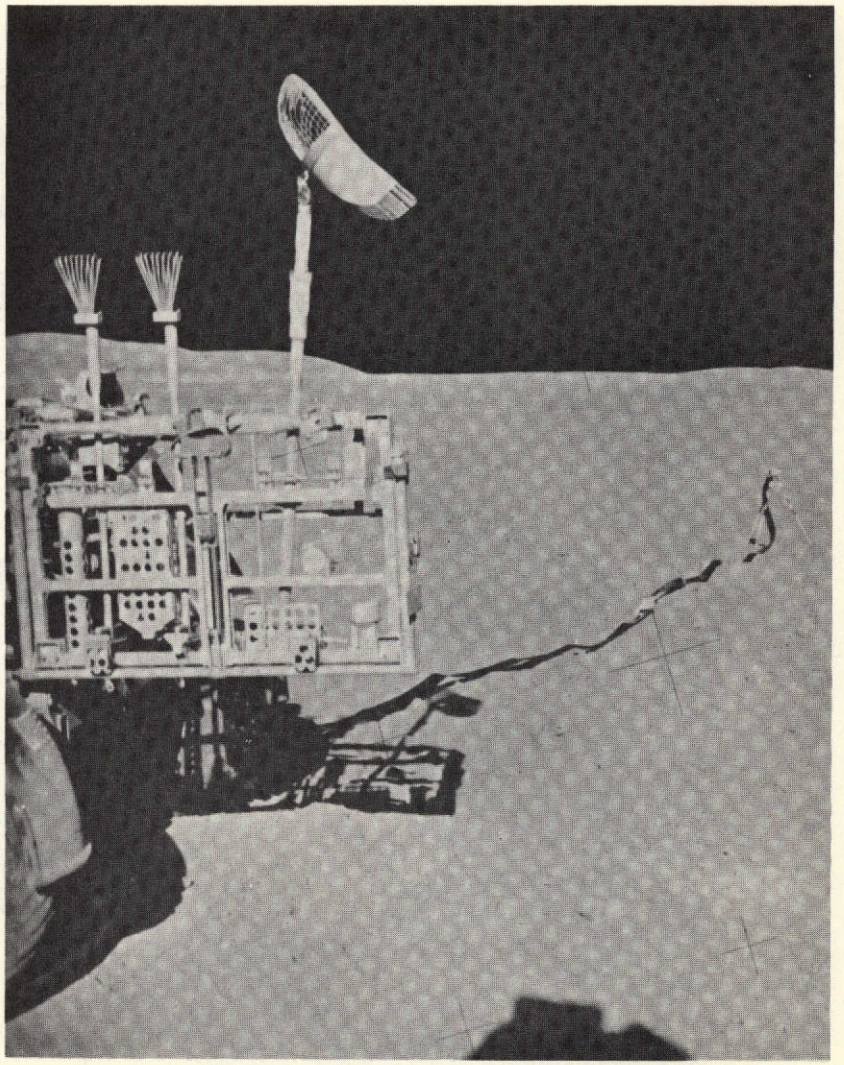

Fig. 3

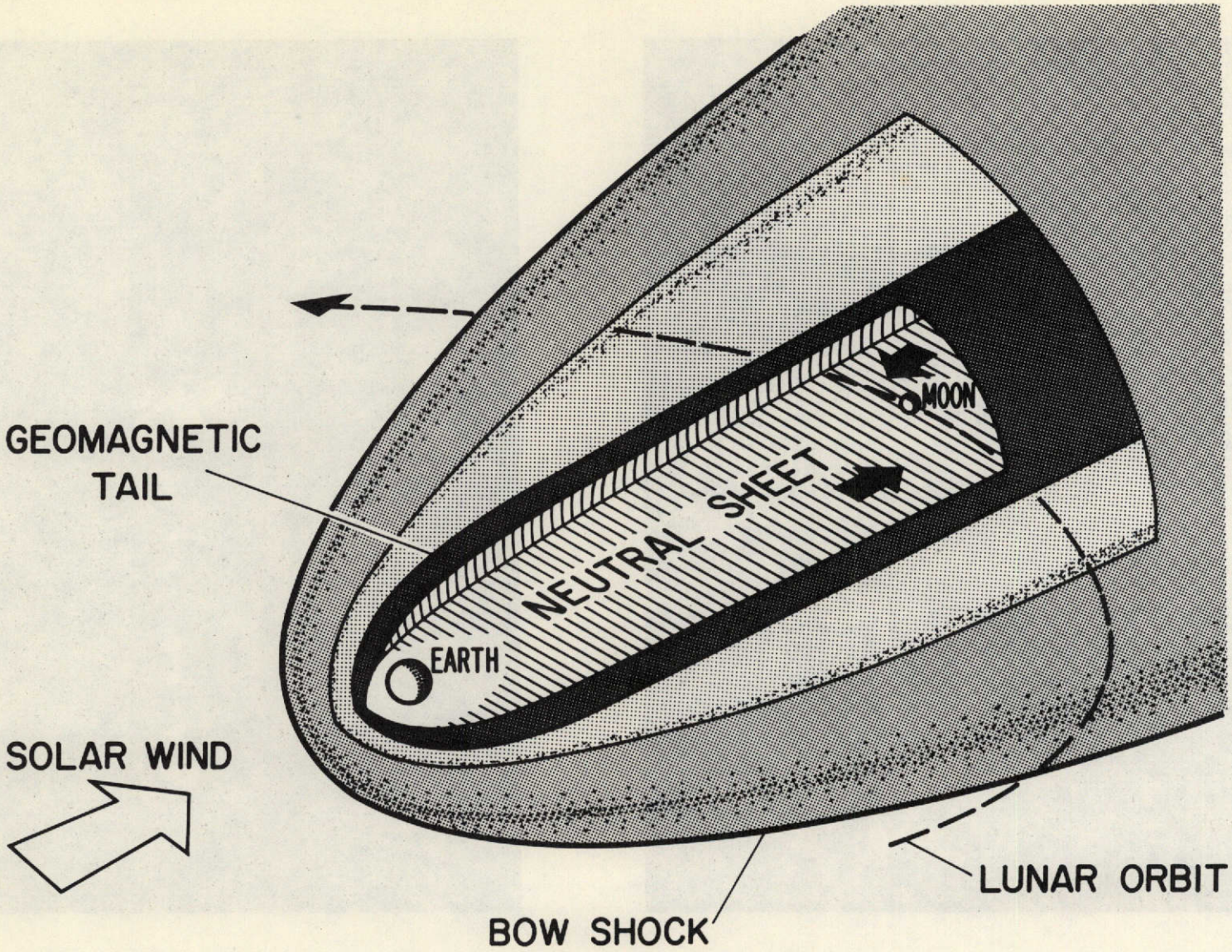

Fig. 4

NATIONAL AERONAUTICS AND SPACE ADMINISTRATION
AMES RESEARCH CENTER, MOFFETT FIELD, CALIFORNIA

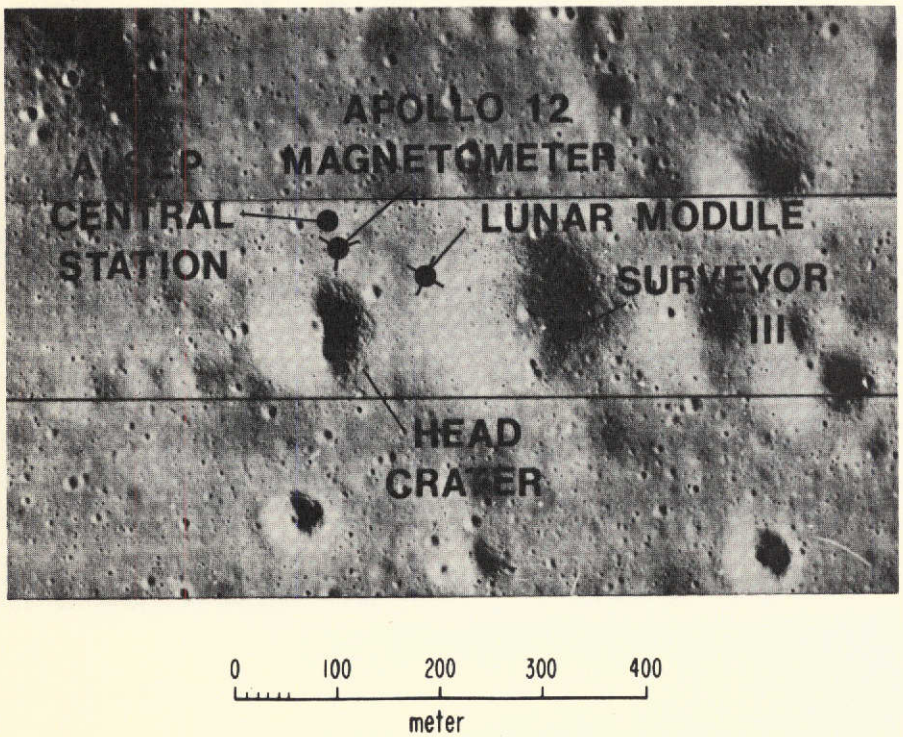
APOLLO 12
MAGNETOMETER
CENTRAL
STATION
LUNAR MODULE
SURVEYOR
III
HEAD
CRATER
0
100
200
300
400
meter

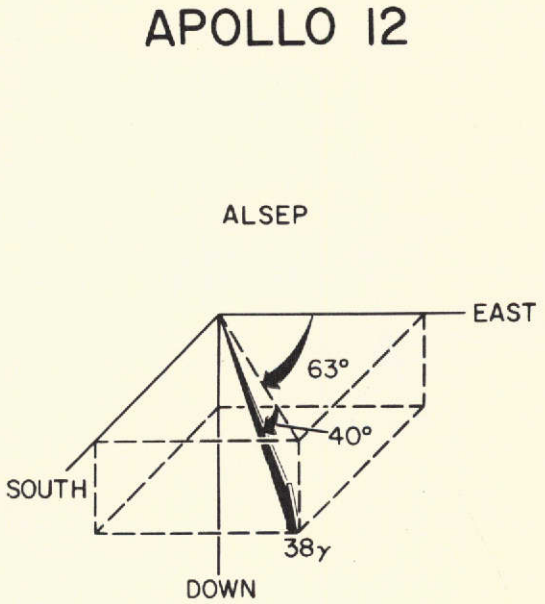
APOLLO 12
ALSEP
EAST
63°
40°
SOUTH
38γ
DOWN

Fig. 5

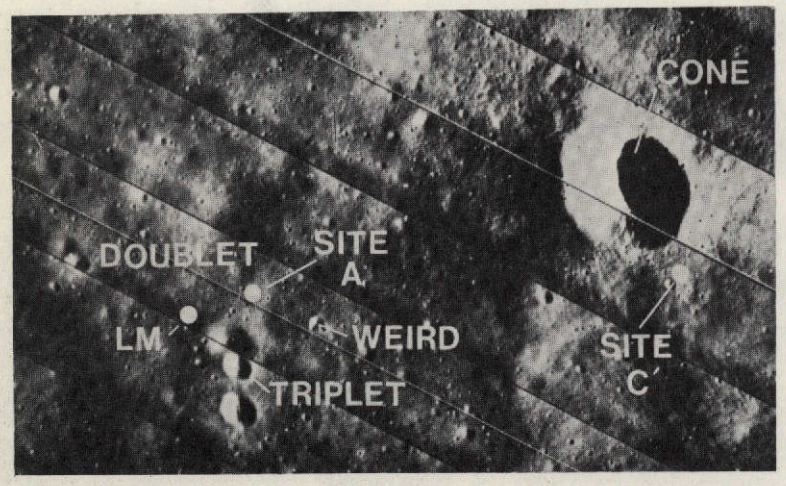
CONE
DOUBLET
SITE A
LM
WEIRD
TRIPLET
SITE C'
0 200 400 600 800 1000
meter

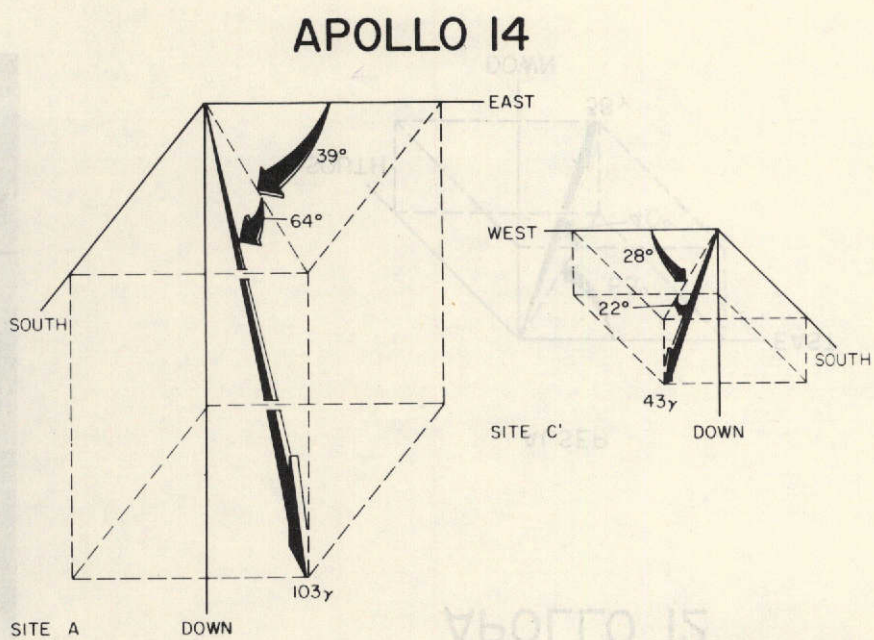
APOLLO 14
EAST
39°
64°
SOUTH
103γ
SITE A
DOWN
WEST
28°
22°
SOUTH
43γ
SITE C'
DOWN

Fig. 6

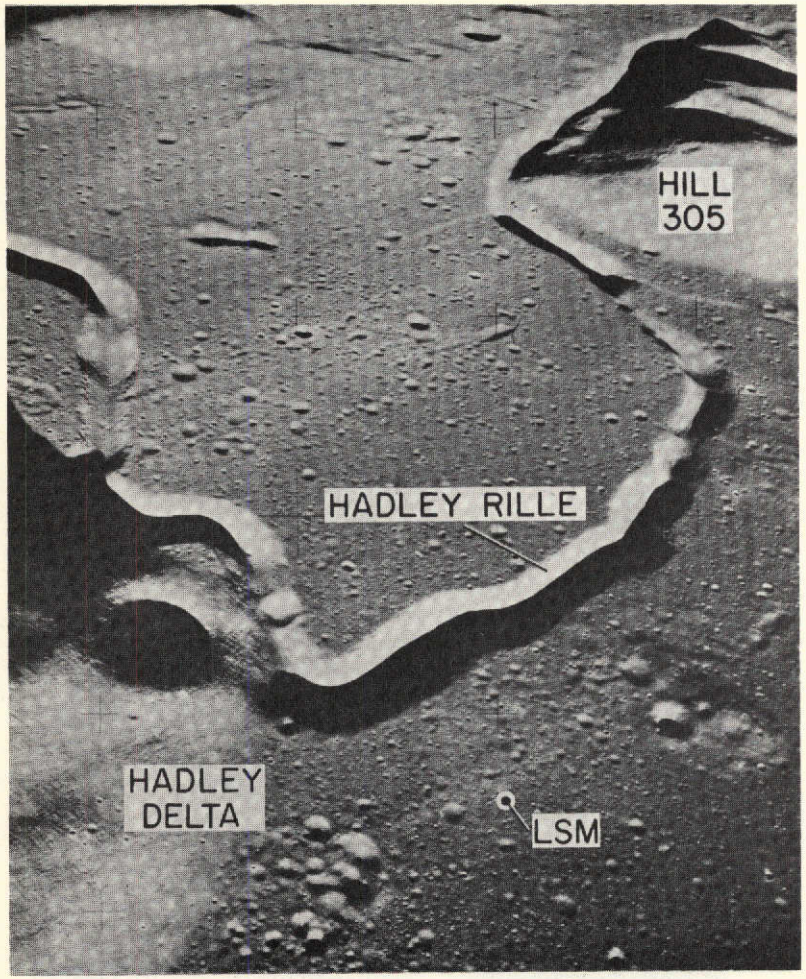
HILL
305
HADLEY RILLE
HADLEY
DELTA
LSM
0
2
4
km

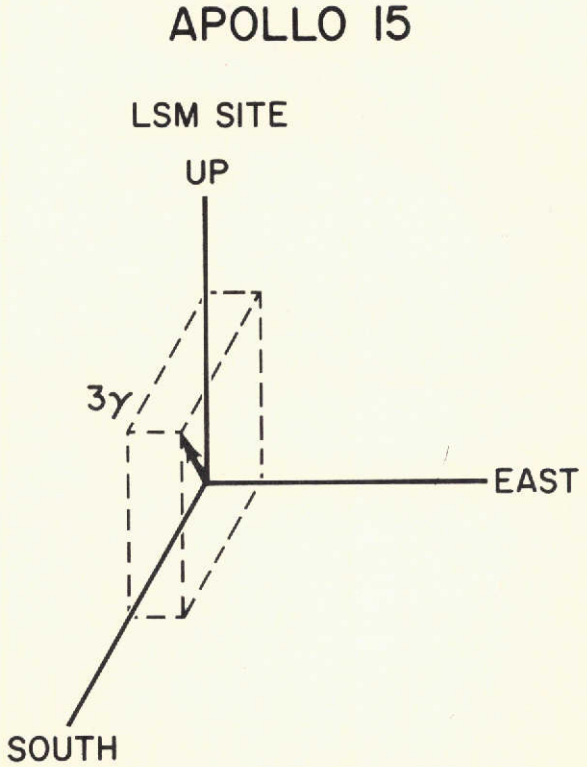
APOLLO 15
LSM SITE
UP
3γ
EAST
SOUTH

Fig. 7

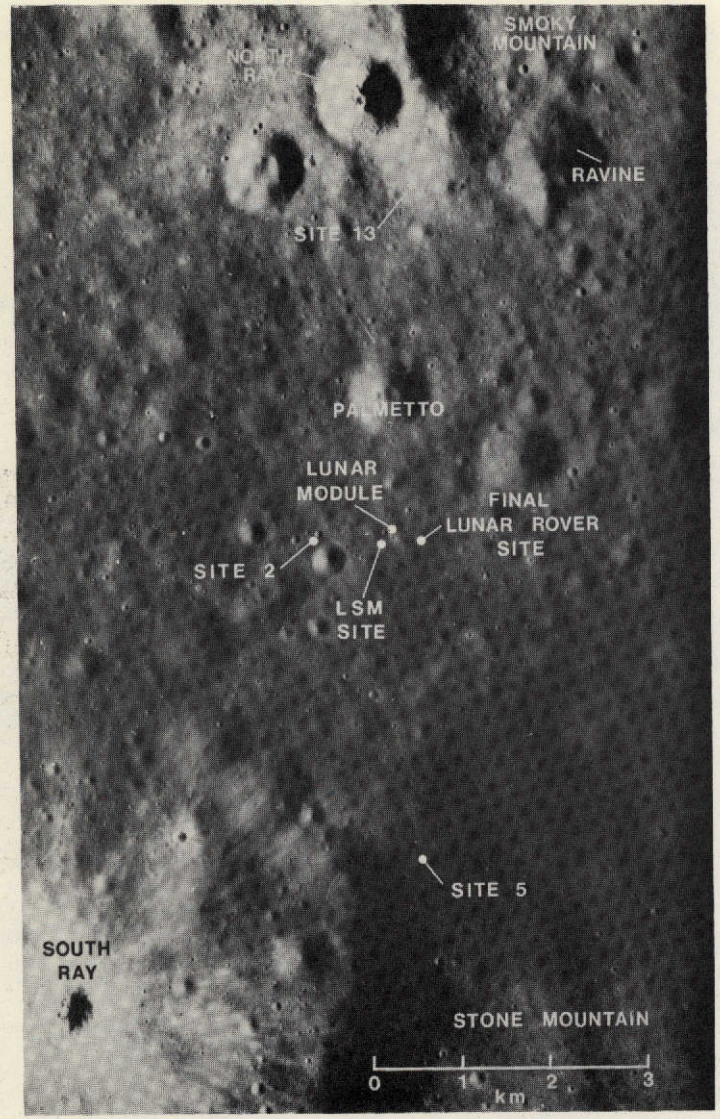
SMOKY MOUNTAIN
RAVINE
SITE 13
PALMETTO
LUNAR MODULE
FINAL LUNAR ROVER SITE
SITE 2
LSM SITE
SITE 5
SOUTH RAY
STONE MOUNTAIN
0
1
2
3
km

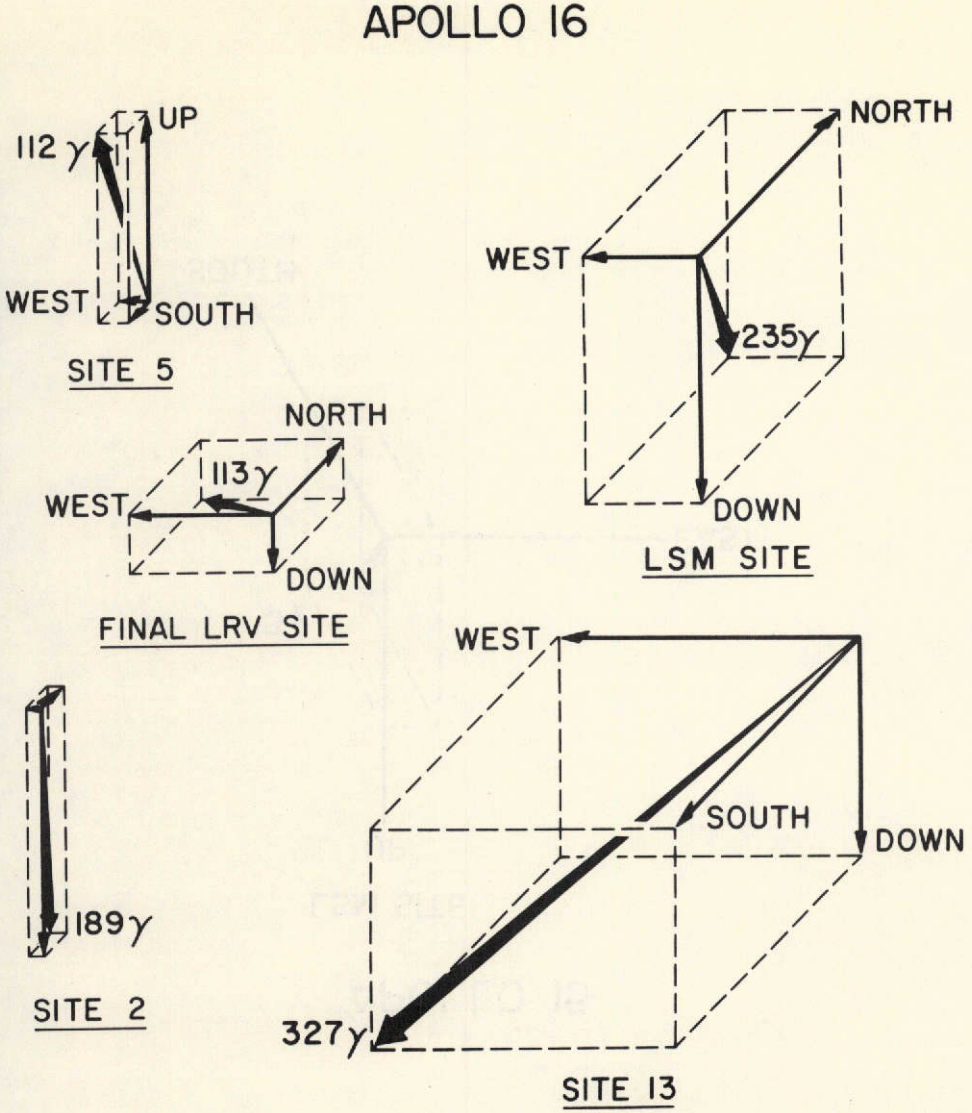
APOLLO 16
112 γ
UP
WEST
SOUTH
SITE 5
NORTH
WEST
235γ
DOWN
LSM SITE
NORTH
113γ
WEST
DOWN
FINAL LRV SITE
189γ
SITE 2
WEST
SOUTH
DOWN
327γ
SITE 13

Fig. 8

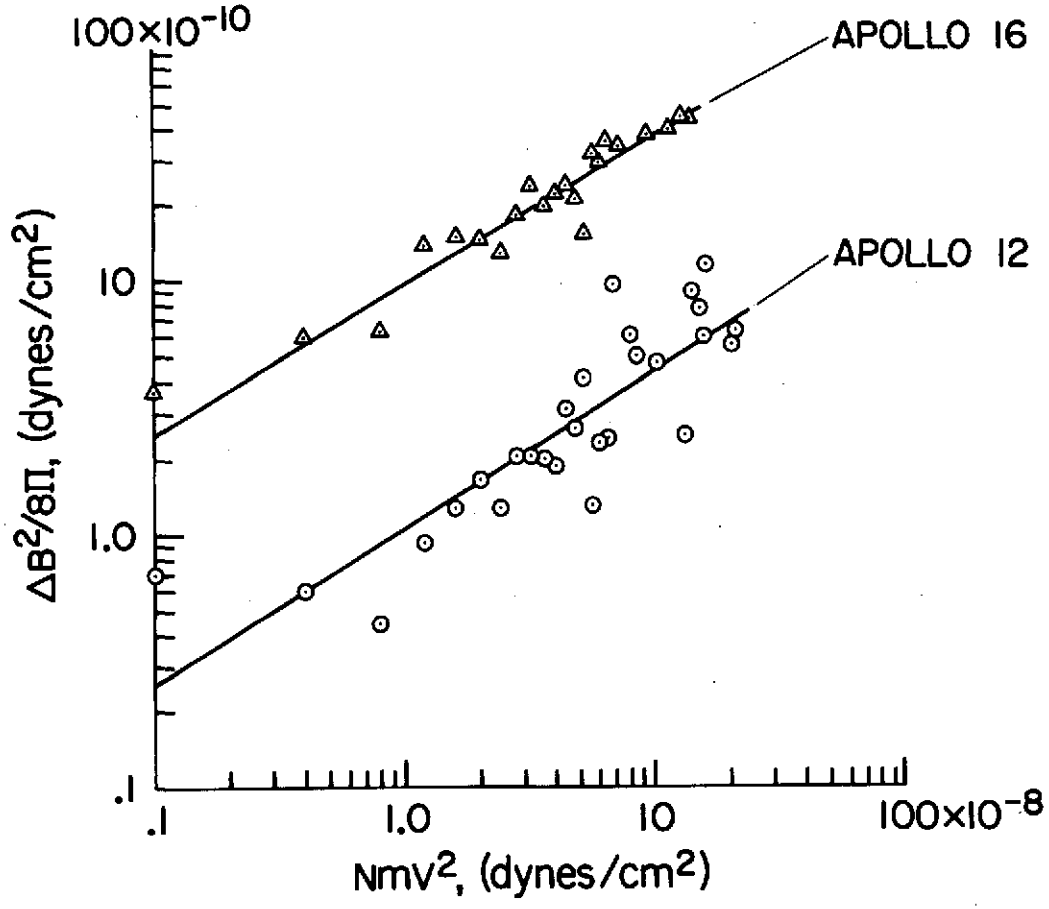
100×10⁻¹⁰
10
1.0
.1
ΔB²/8Π, (dynes/cm²)
APOLLO 16
APOLLO 12
.1
1.0
10
100×10⁻⁸
Nmv², (dynes/cm²)

Fig. 9

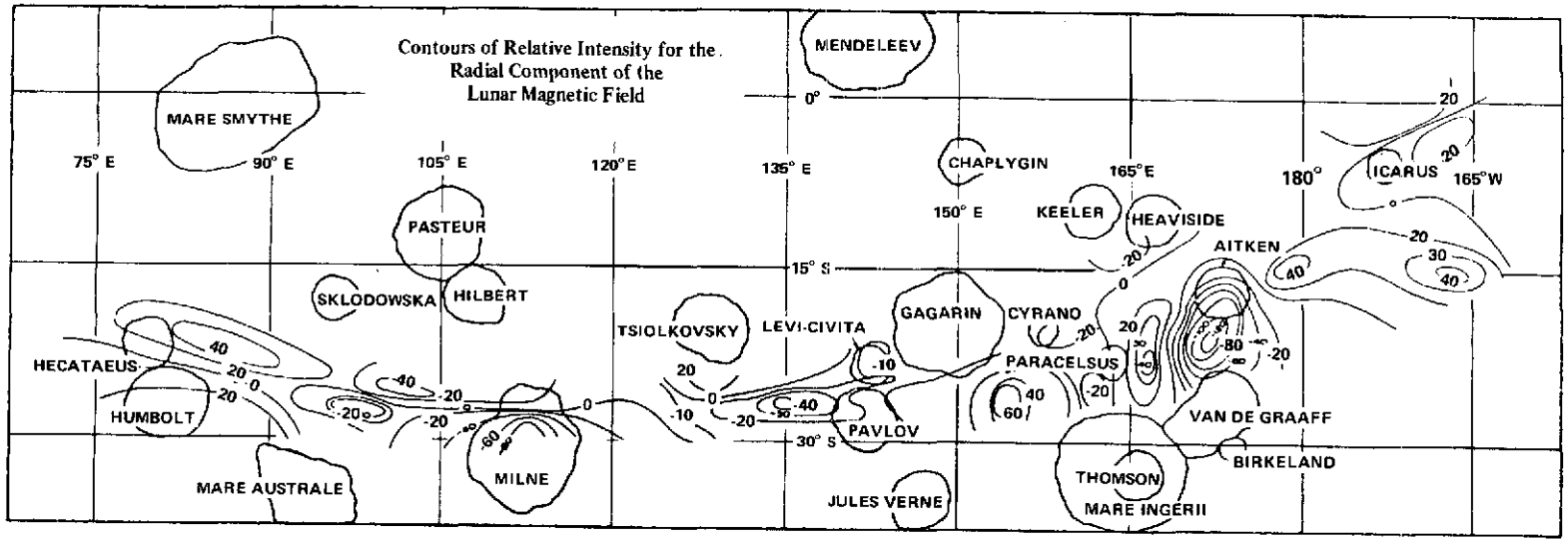
Contours of Relative Intensity for the
Radial Component of the
Lunar Magnetic Field
MENDELEEV
MARE SMYTHE
CHAPLYGIN
ICARUS
PASTEUR
KEELER
HEAVISIDE
AITKEN
SKLODOWSKA
HILBERT
TSIOLKOVSKY
LEVI-CIVITA
GAGARIN
CYRANO
PARACELSUS
HECATAEUS
HUMBOLT
PAVLOV
VAN DE GRAAFF
BIRKELAND
MILNE
MARE AUSTRALE
JULES VERNE
THOMSON
MARE INGERII
0°
15° S
30° S
75° E
90° E
105° E
120° E
135° E
150° E
165° E
180°
165° W

Fig. 10

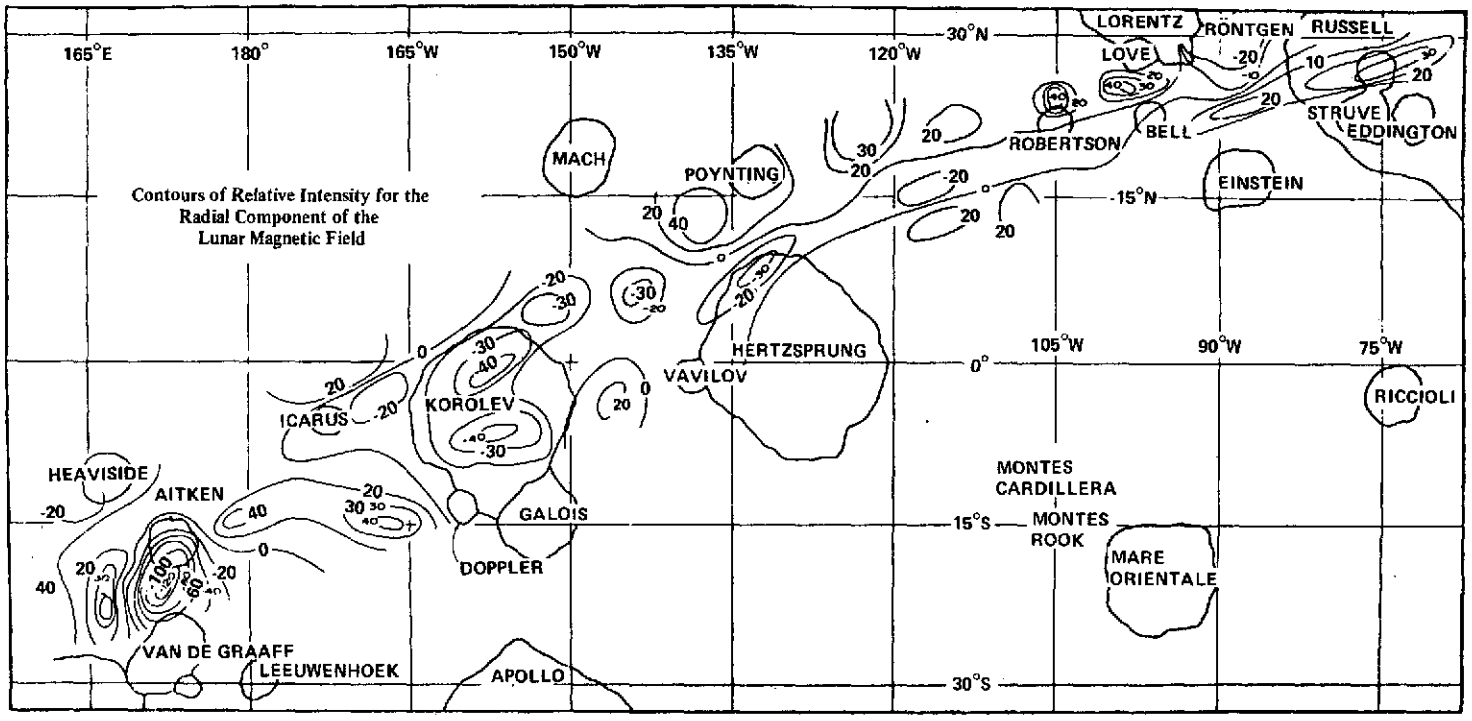
Contours of Relative Intensity for the
Radial Component of the
Lunar Magnetic Field
165°E
180°
165°W
150°W
135°W
120°W
105°W
90°W
75°W
30°N
15°N
0°
15°S
30°S
LORENTZ
RÖNTGEN
RUSSELL
LOVE
ROBERTSON
BELL
STRUVE
EDDINGTON
EINSTEIN
MACH
POYNTING
HERTZSPRUNG
VAVILOV
RICCIOLI
ICARUS
KOROLEV
HEAVISIDE
AITKEN
GALOIS
DOPPLER
MONTES
CARDILLERA
MONTES
ROOK
MARE
ORIENTALE
VAN DE GRAAFF
LEEUWENHOEK
APOLLO

Fig. 11

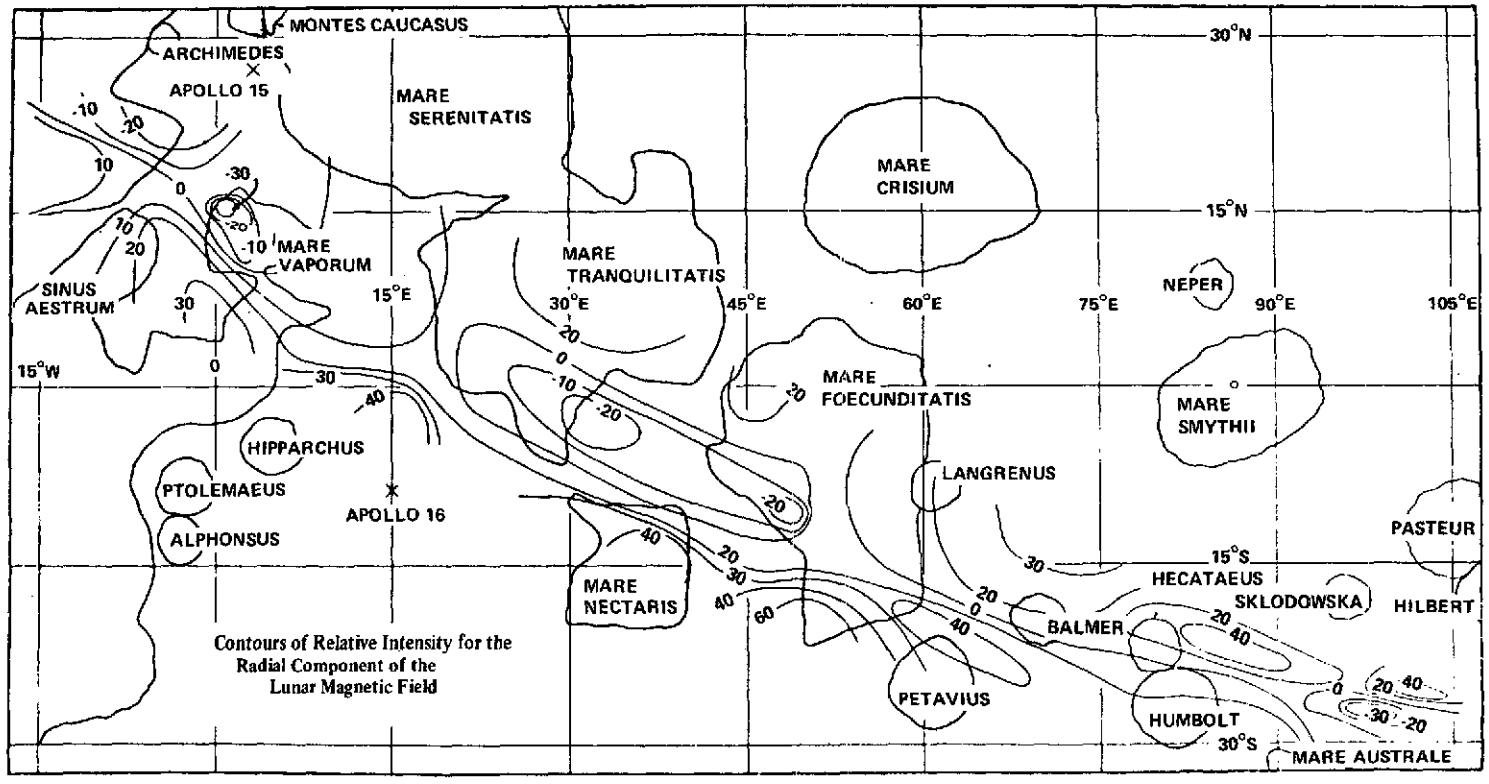
MONTES CAUCASUS
ARCHIMEDES
APOLLO 15
MARE SERENITATIS
MARE CRISIUM
MARE VAPORUM
MARE TRANQUILITATIS
SINUS AESTRUM
NEPER
MARE FOECUNDITATIS
MARE SMYTHII
HIPPARCHUS
PTOLEMAEUS
ALPHONSUS
APOLLO 16
LANGRENUS
PASTEUR
MARE NECTARIS
HECATAEUS
SKLODOWSKA
HILBERT
BALMER
PETAVIUS
HUMBOLT
MARE AUSTRALE
30°N
15°N
15°S
30°S
15°W
15°E
30°E
45°E
60°E
75°E
90°E
105°E
Contours of Relative Intensity for the Radial Component of the Lunar Magnetic Field

Fig. 12

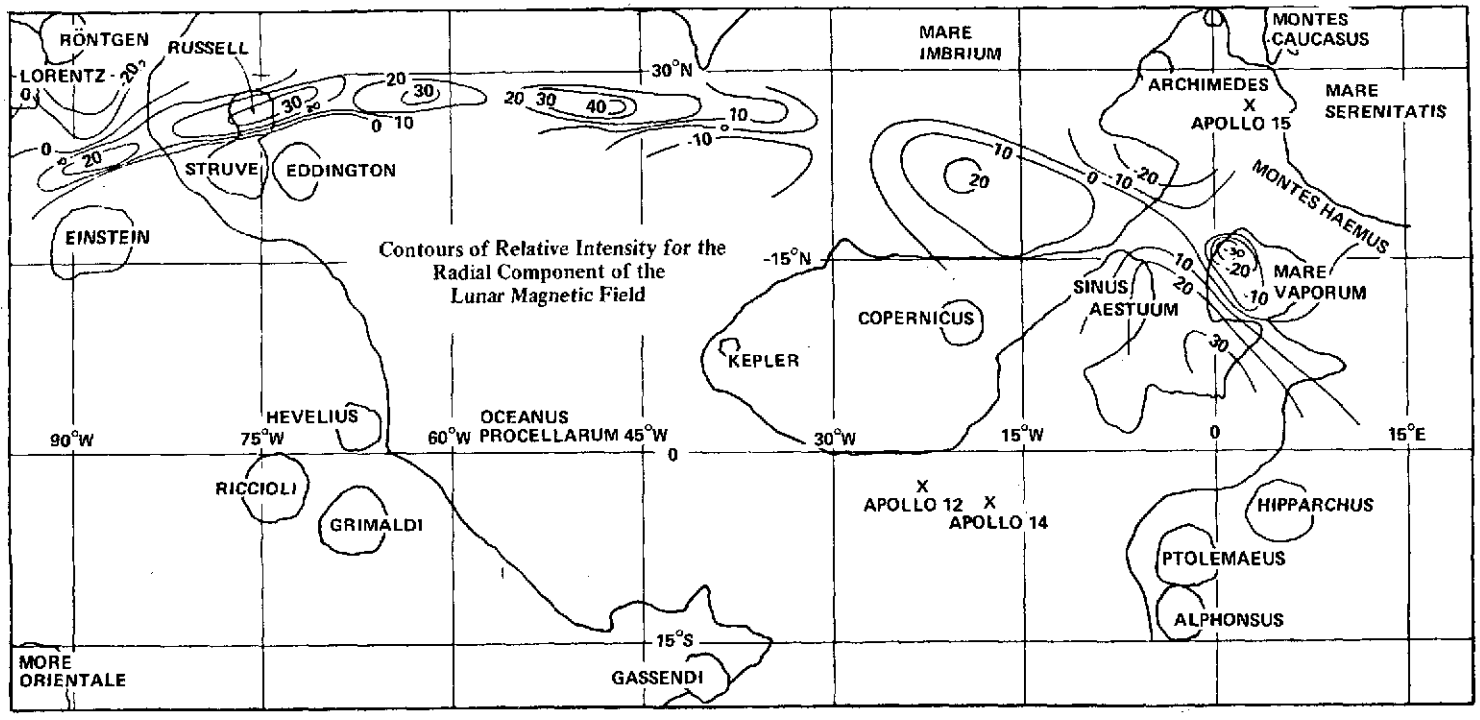
Contours of Relative Intensity for the
Radial Component of the
Lunar Magnetic Field
RÖNTGEN
RUSSELL
LORENTZ
STRUVE
EDDINGTON
EINSTEIN
HEVELIUS
RICCIOLI
GRIMALDI
OCEANUS PROCELLARUM
MARE IMBRIUM
MONTES CAUCASUS
ARCHIMEDES
APOLLO 15
MARE SERENITATIS
MONTES HAEMUS
SINUS AESTUUM
MARE VAPORUM
COPERNICUS
KEPLER
APOLLO 12
APOLLO 14
HIPPARCHUS
PTOLEMAEUS
ALPHONSUS
GASSENDI
MORE ORIENTALE
30°N
-15°N
15°S
90°W
75°W
60°W
45°W
30°W
15°W
0
15°E

Fig. 13

(a)
LARGE SOLAR
OR TERRESTRIAL
FIELD

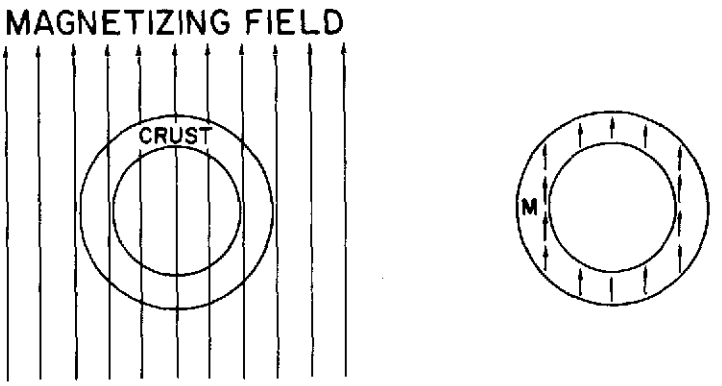

(b)
ANCIENT
MAGNETIZED
CORE

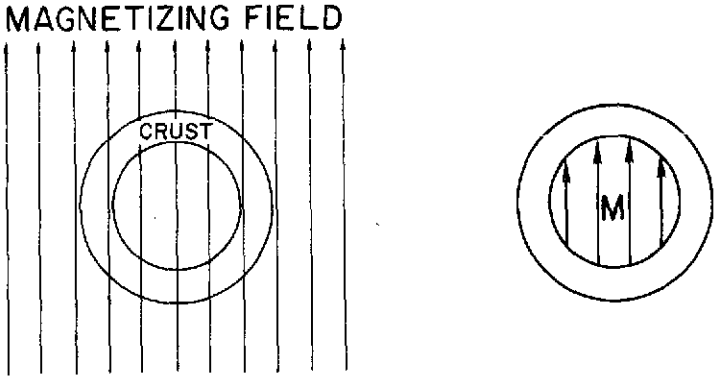

(c)
IRON CORE
DYNAMO

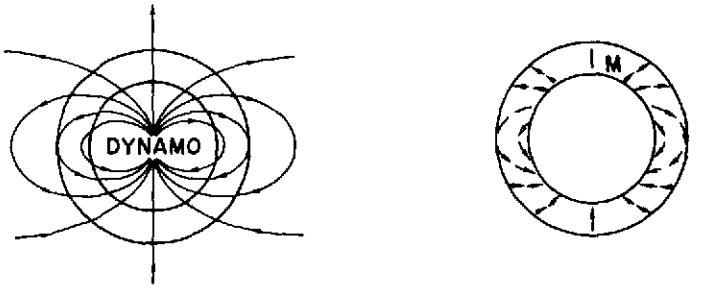

Fig. 14

(a)
SHALLOW
Fe-FeS DYNAMO

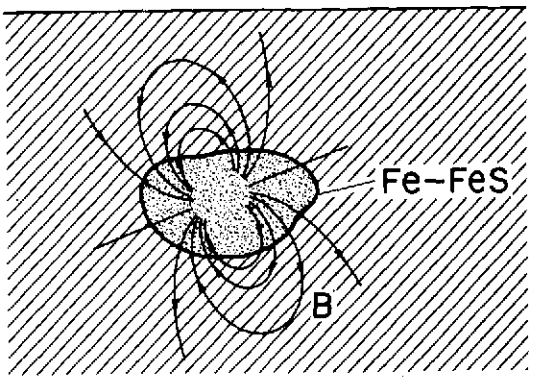

(b)
LOCAL INDUCED
UNIPOLAR DYNAMO

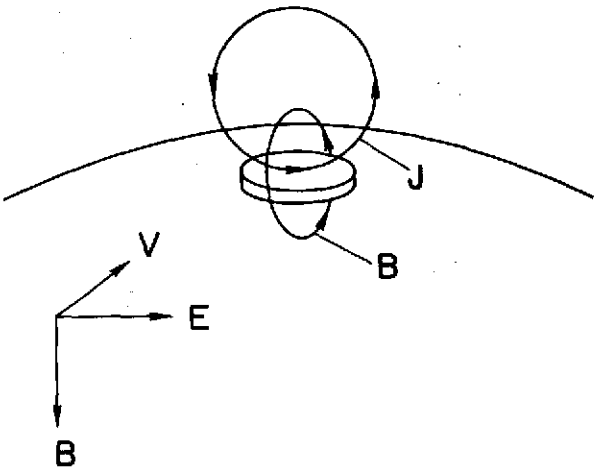

(c)
LOCAL
THERMOELECTRIC
DYNAMO

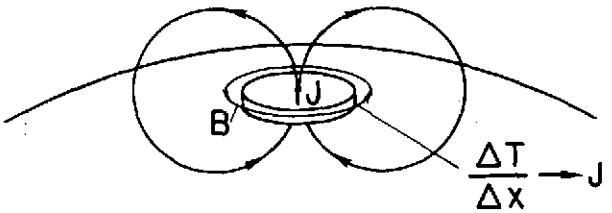

(d)
SHOCK
MAGNETIZATION

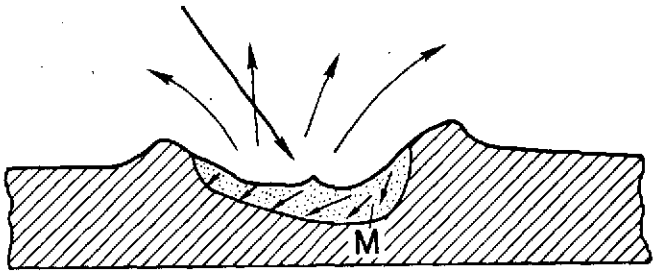

Fig. 15

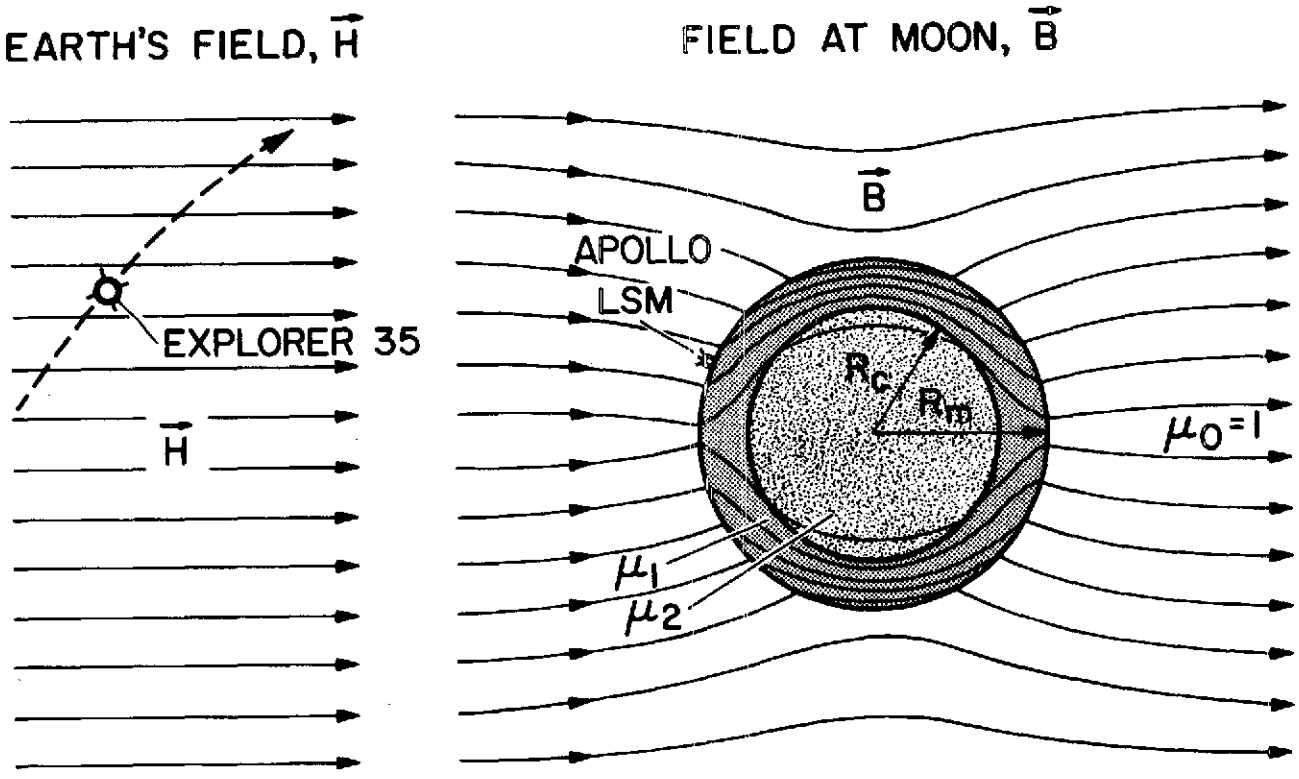

Fig. 16

NATIONAL AERONAUTICS AND SPACE ADMINISTRATION
AMES RESEARCH CENTER, MOFFETT FIELD, CALIFORNIA

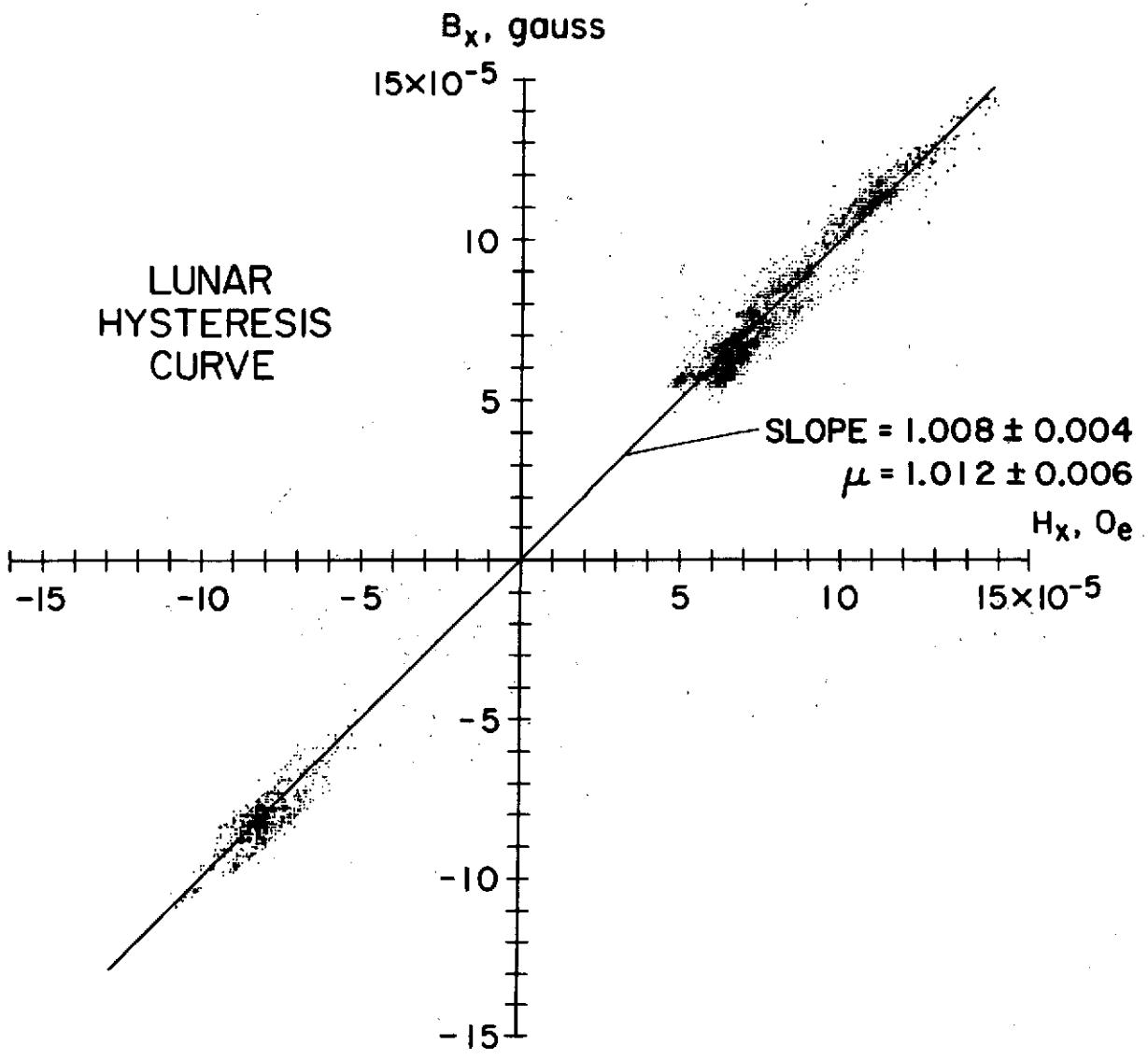

Fig. 17

NATIONAL AERONAUTICS AND SPACE ADMINISTRATION
AMES RESEARCH CENTER, MOFFETT FIELD, CALIFORNIA

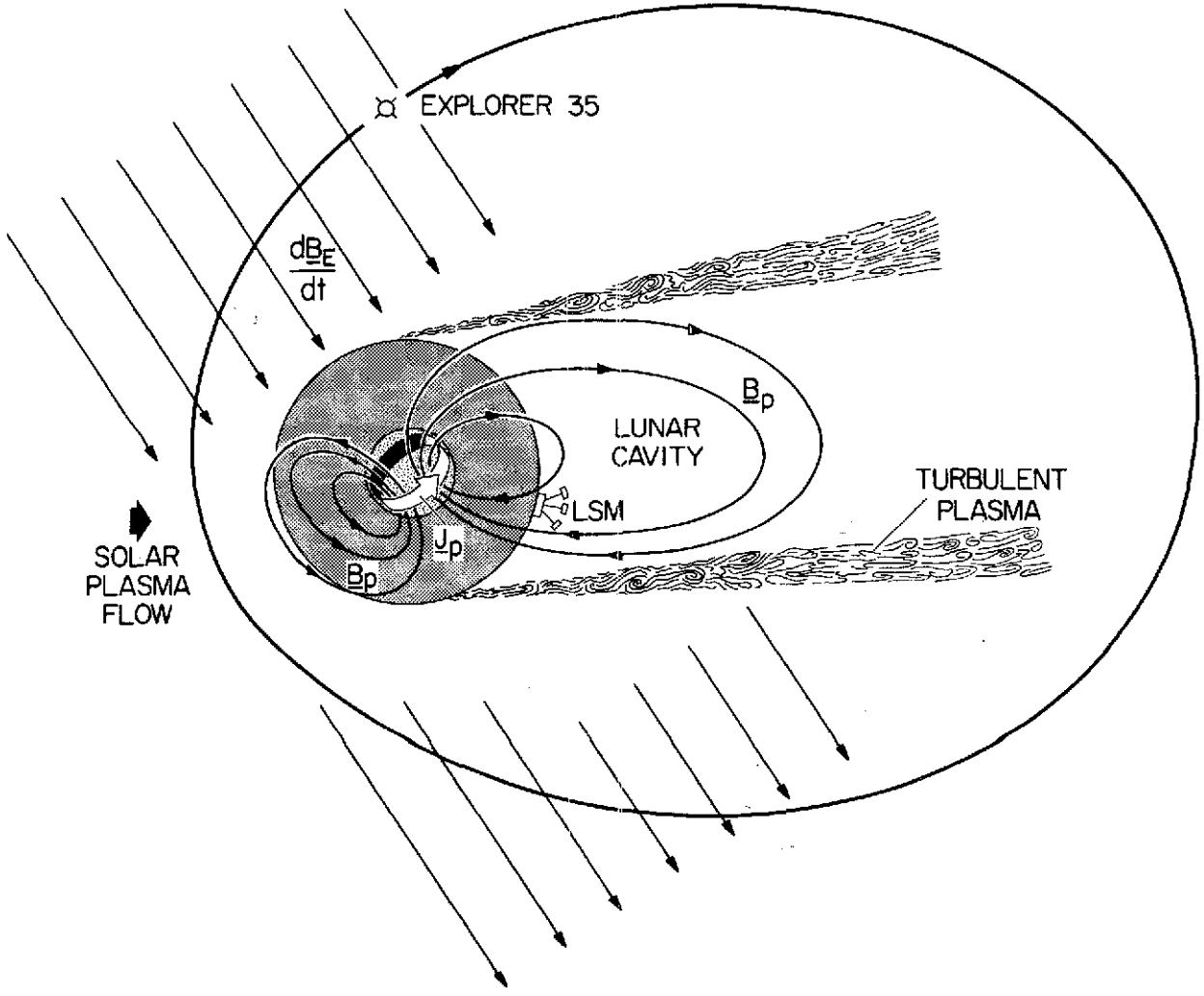
EXPLORER 35
$\frac{d\underline{B}_E}{dt}$
$\underline{B}_p$
LUNAR
CAVITY
TURBULENT
PLASMA
LSM
$\underline{J}_p$
$\underline{B}_p$
SOLAR
PLASMA
FLOW

Fig. 18

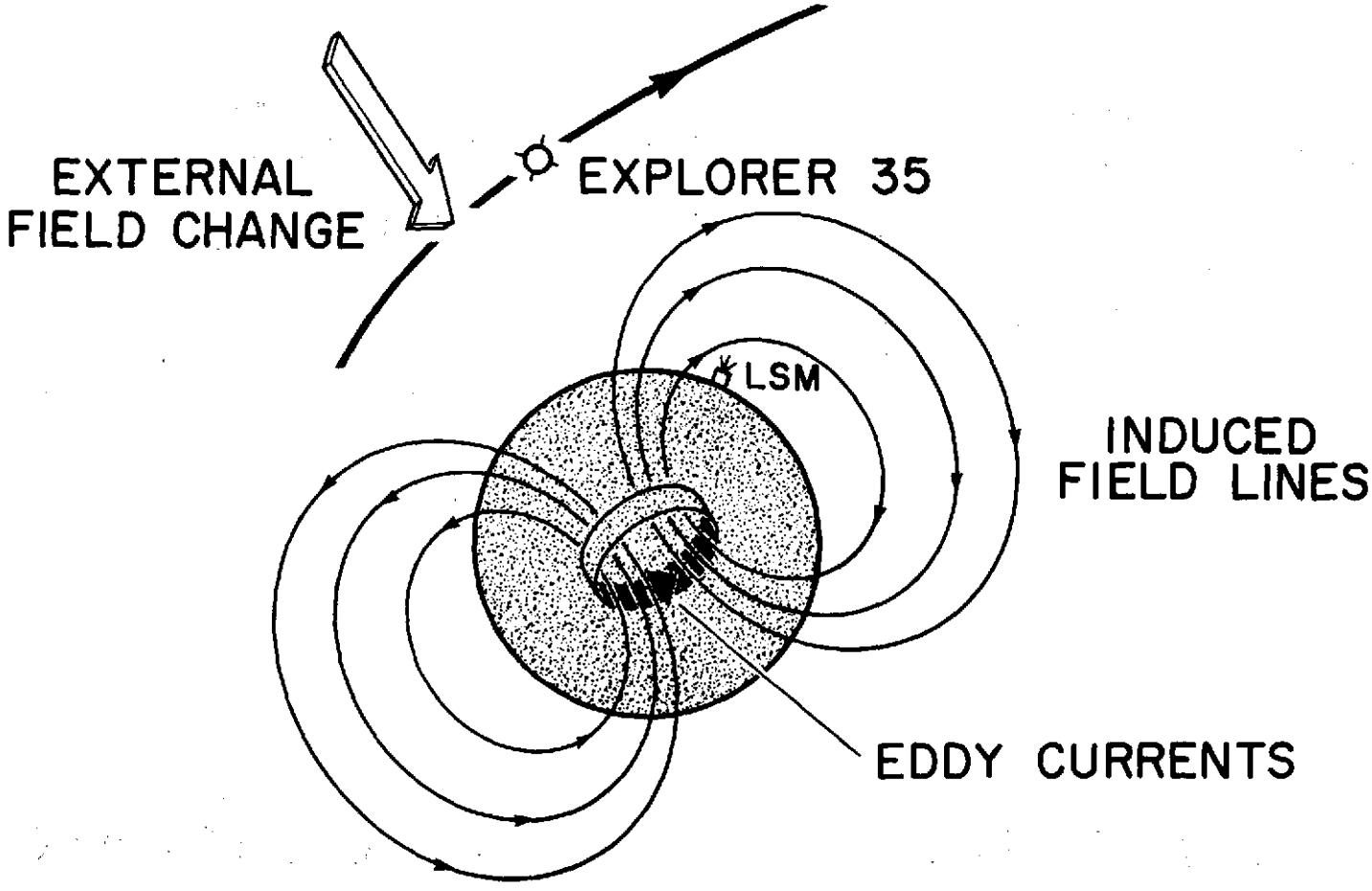
EXTERNAL
FIELD CHANGE
EXPLORER 35
LSM
INDUCED
FIELD LINES
EDDY CURRENTS

Fig. 19

NIGHTSIDE DATA

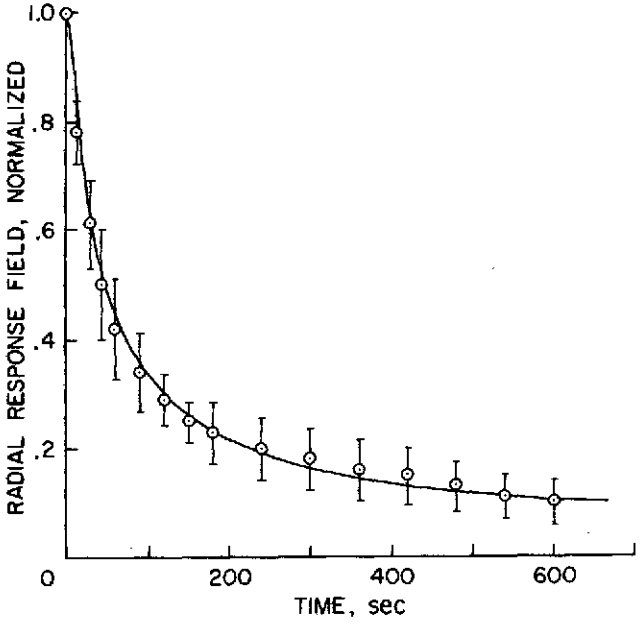

DAYSIDE DATA

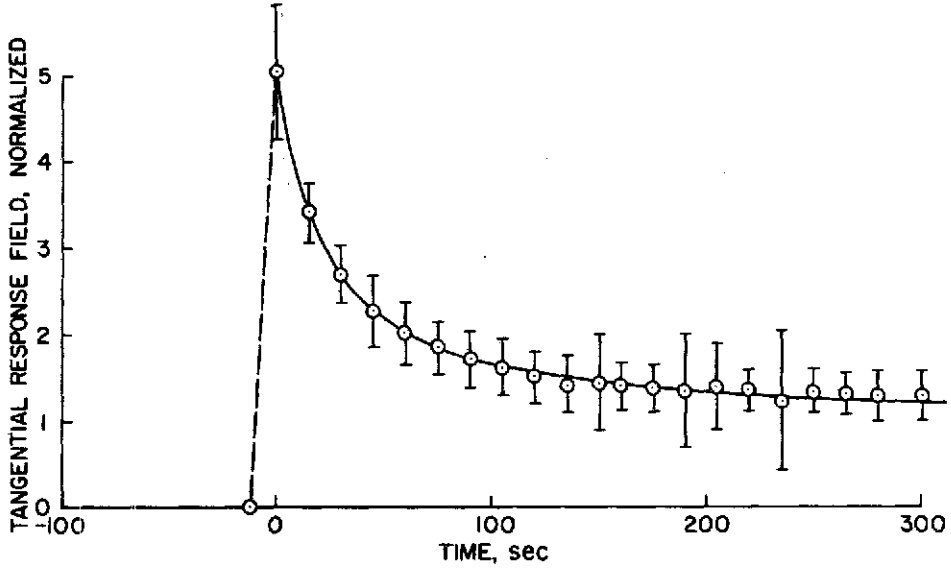

Fig. 20

GEOMAGNETIC TAIL TRANSIENT RESPONSE

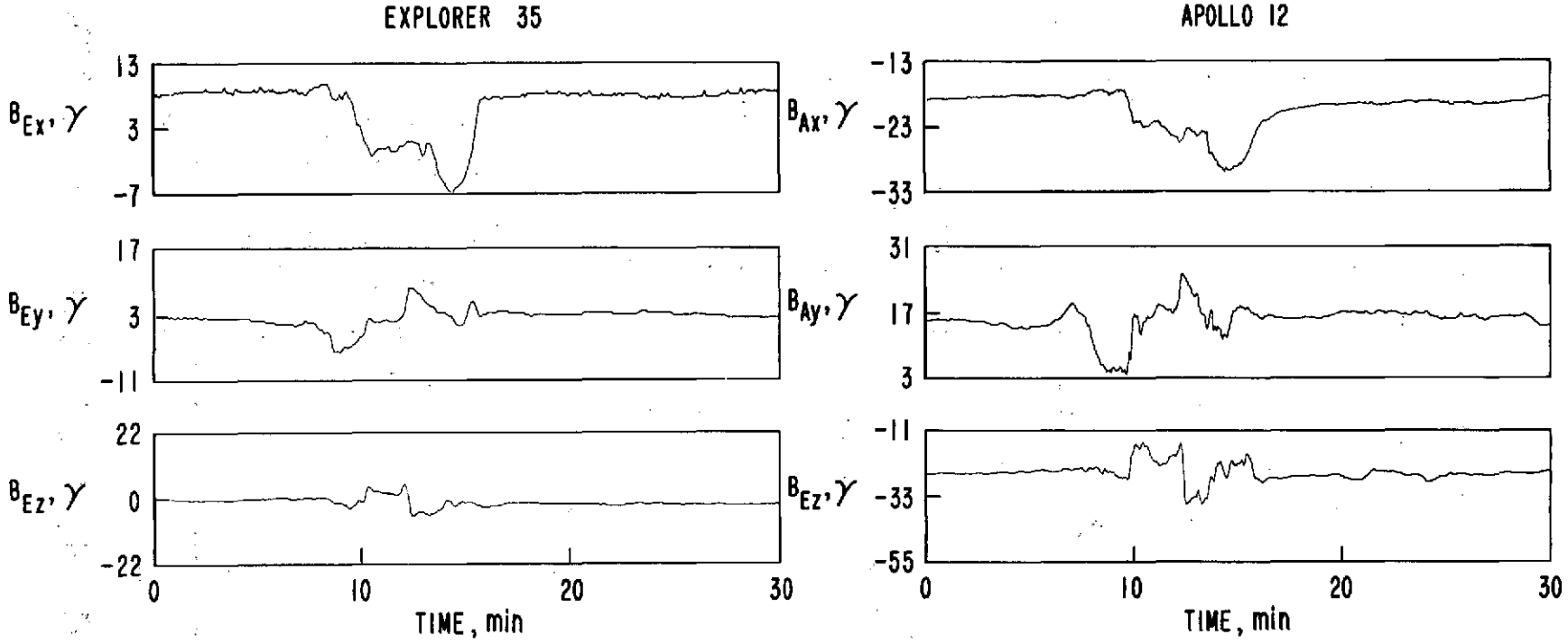

Fig. 21

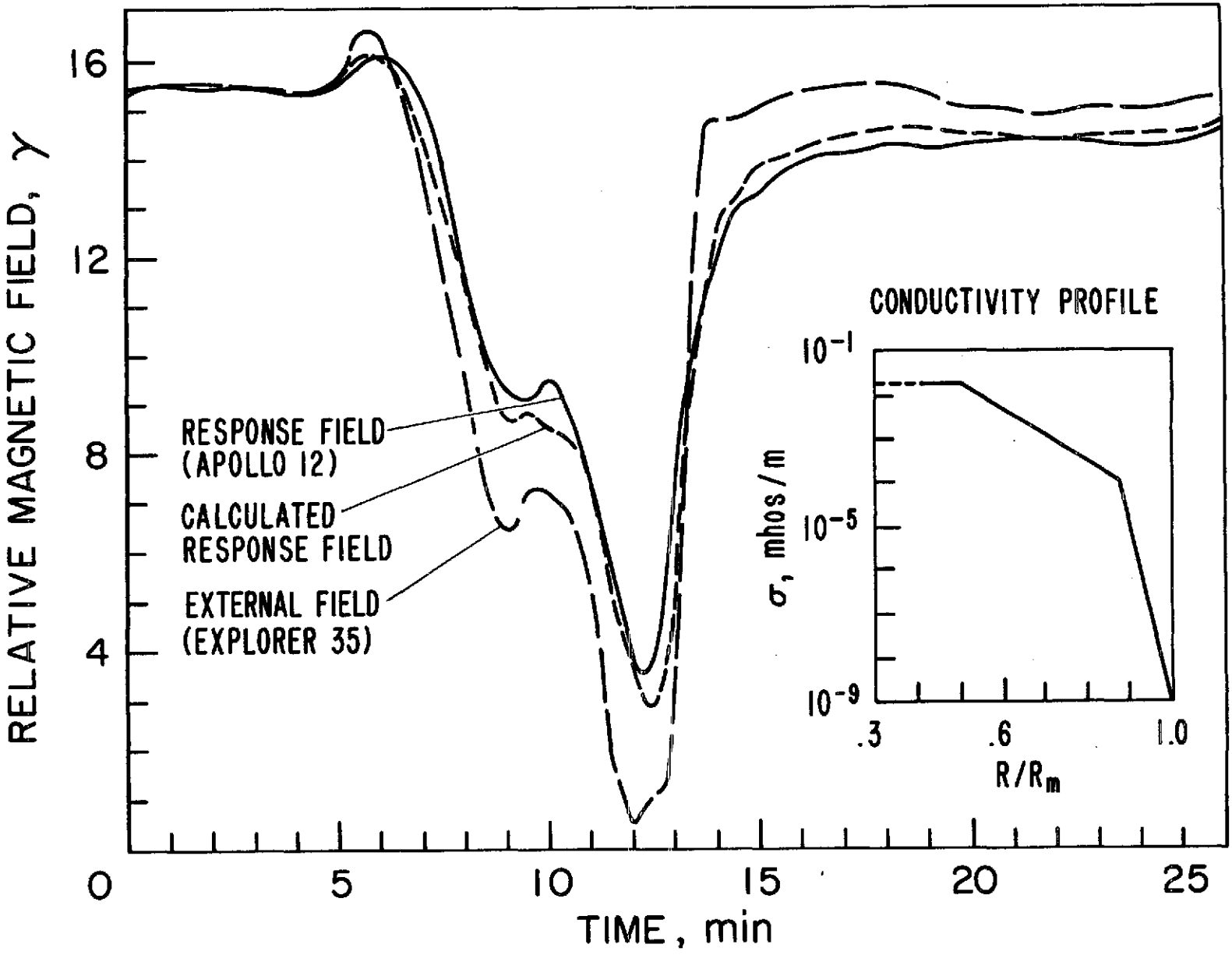
RELATIVE MAGNETIC FIELD, γ
16
12
8
4
0
5
10
15
20
25
TIME, min
RESPONSE FIELD
(APOLLO 12)
CALCULATED
RESPONSE FIELD
EXTERNAL FIELD
(EXPLORER 35)
CONDUCTIVITY PROFILE
10⁻¹
10⁻⁵
10⁻⁹
σ, mhos/m
.3
.6
1.0
R/Rm

Fig. 22

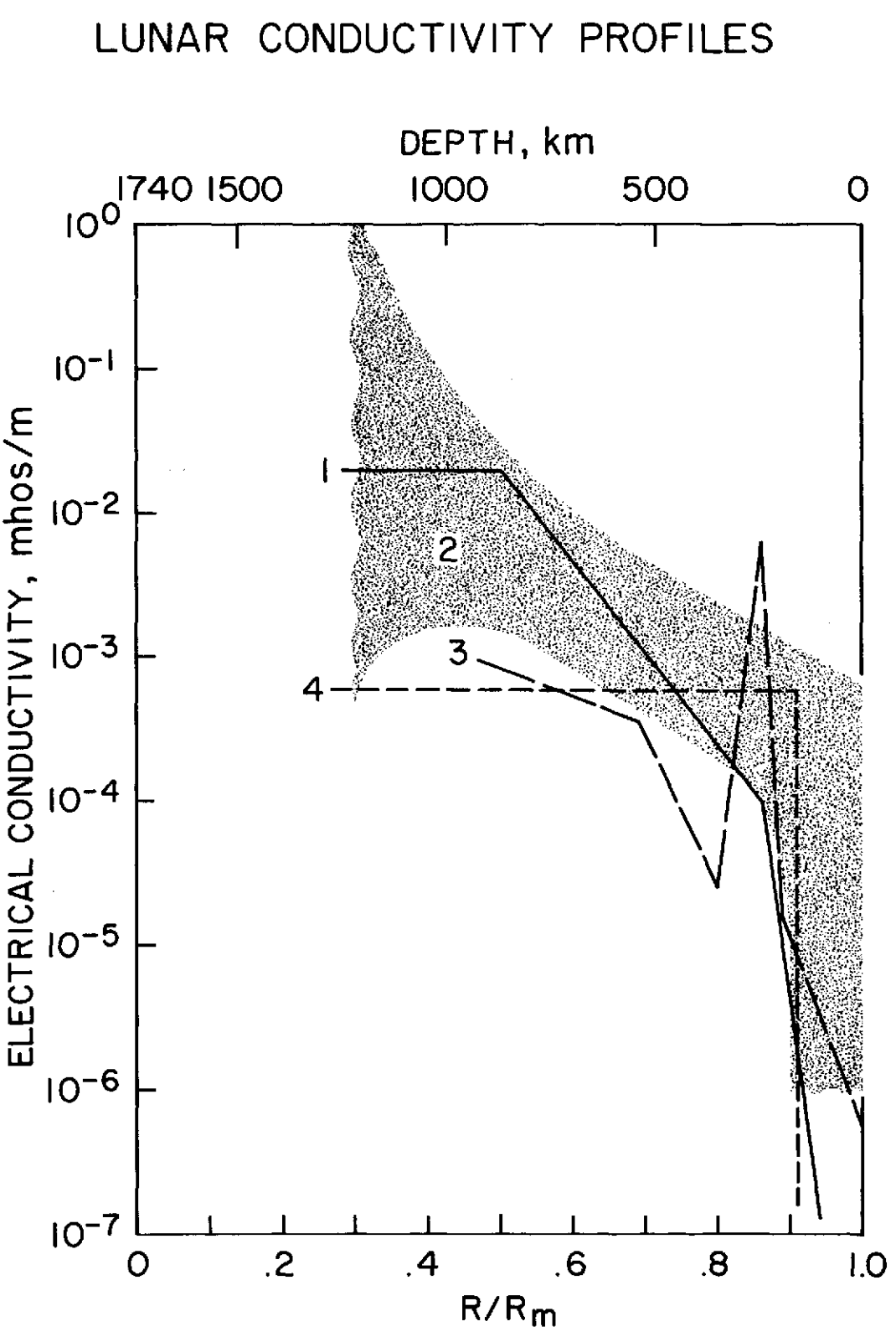
LUNAR CONDUCTIVITY PROFILES
DEPTH, km
1740 1500
1000
500
0
10^{0}
10^{-1}
10^{-2}
10^{-3}
10^{-4}
10^{-5}
10^{-6}
10^{-7}
ELECTRICAL CONDUCTIVITY, mhos/m
1
2
3
4
0
.2
.4
.6
.8
1.0
R/Rm

Fig. 23

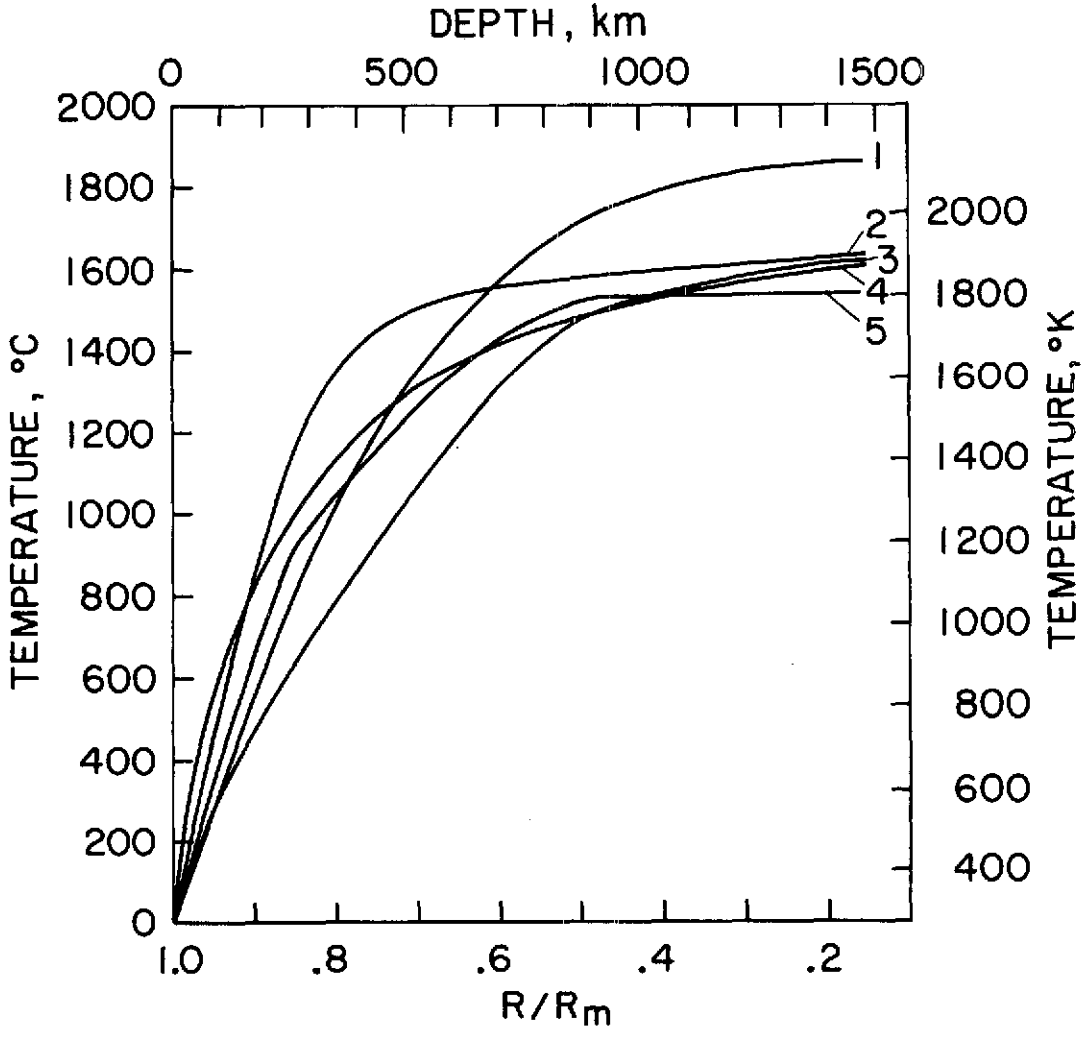
DEPTH, km
0
500
1000
1500
2000
1800
1600
1400
1200
1000
800
600
400
200
0
TEMPERATURE, °C
TEMPERATURE, °K
1
2
3
4
5
1.0
.8
.6
.4
.2
R/Rm

Fig. 24